

# COYOTES I: the photometric variability and rotational evolution of T Tauri stars<sup>\*</sup>

J. Bouvier<sup>1</sup>, S. Cabrit<sup>1</sup>, M. Fernández<sup>2</sup>, E.L. Martín<sup>3</sup>, and J.M. Matthews<sup>4,5</sup>

<sup>1</sup> Laboratoire d'Astrophysique, Observatoire de Grenoble, Université Joseph Fourier, B.P. 53X, F-38041 Grenoble Cedex, France

<sup>2</sup> Departamento de Física Teórica, C-XI, Facultad de Ciencias, Universidad Autónoma de Madrid, Ciudad Universitaria de Cantoblanco, E-28049 Madrid, Spain

<sup>3</sup> Instituto de Astrofísica de Canarias, E-38200 La Laguna, Tenerife, Spain

<sup>4</sup> Department of Geophysics and Astronomy, University of British Columbia, Vancouver, B.C., V6T 1Z4, Canada

<sup>5</sup> Département de Physique, Université de Montréal, C.P. 6128, Succ. A, Montréal, Québec, H3C 3J7, Canada

Received November 17, 1992; accepted January 4, 1993

**Abstract.** In a multi-site photometric campaign to monitor T Tauri stars (TTS) in the Taurus-Auriga cloud over more than two months – dubbed Coordinated Observations of Young Objects from Earthbound Sites (COYOTES) –, we find all 24 of our target stars show evidence for *periodic* light variations with periods between 1.2 and 24.0 days. This more than doubles the number of periods published for Tau-Aur TTS. The variations of 20 of these stars can be interpreted as rotational modulation of the stellar flux by surface spots. The periods of the four remaining stars (RY Tau, BD+24°676, TAP 26, and LkCa-21) may correspond to orbital periods of binary systems. Models of the UBVRI light curves lead to the properties of the spots, both hotter and cooler than the photospheric temperature, which appear to be the principal source of the photometric variability of TTS on timescales of days and weeks.

The longest rotational period we measure (12 d, for GM Aur) leads to an equatorial velocity of  $8 \text{ km s}^{-1}$ , which confirms the paucity of extremely slow rotators ( $V_{eq} \ll 10 \text{ km s}^{-1}$ ) among TTS younger than  $5 \times 10^6$  yrs. Combining our 20 rotational periods with those published for 17 other Tau-Aur TTS, we find that the Weak-line TTS ( $EW(H_\alpha) < 10 \text{ \AA}$ ) rotate faster than Classical TTS ( $EW(H_\alpha) \geq 10 \text{ \AA}$ ) at the 99.9% confidence level (according to a K-S test). The mean rotational period for the 11 WTTS is  $4.1 \pm 1.7$  d; for the 15 CTTS,  $7.6 \pm 2.1$  d. We interpret this difference as evidence that WTTS spin-up as they contract on their convective tracks, while CTTS are prevented from doing so by either (a) their strong winds carrying away excess angular momentum and/or (b) a magnetic coupling between the stars and their inner accretion disks, as suggested by recent models. We discuss the implications of this interpretation

for the subsequent evolution of TTS toward the main sequence. In particular, we propose that the different rotational histories of WTTS and CTTS on their convective tracks may account for the large range of rotational velocities observed among low-mass dwarfs in young clusters.

**Key words:** stars: pre-main sequence – stars: rotation – stars: activity

## 1. Introduction

Solar-type stars have long been known to exhibit small and uniform rotational velocities on the main sequence. The idea of rotational braking of late-type stars on the main sequence by magnetic winds was first introduced by Schatzman (1962) and later supported by the observations of Kraft (1967) and Skumanich (1972). More recent theoretical models of the evolution of the angular momentum of solar-mass stars confirm these pioneering works and indicate that the surface velocity of low-mass dwarfs becomes independent of the initial angular momentum after a few  $10^8$  yr spent on the main sequence (e.g. Endal & Sofia 1981). Clues to the initial angular momentum distribution in solar-type stars are therefore to be obtained from the study of the rotation rates of much younger stars such as T Tauri stars (TTS) that are low-mass pre-main sequence (PMS) stars with an age less than  $10^7$  yr. Besides, the rotation rates of TTS are expected to be influenced by the violent mass-accretion and mass-loss phenomena that take place during this phase of stellar evolution. Therefore, the rotational properties of TTS bring insight into the processes by which the young star exchanges angular momentum with its circumstellar environment.

A large amount of work has been devoted in the last 10 years to determine the rotational velocities of TTS. Most studies

Send offprint requests to: J. Bouvier

<sup>\*</sup> Based on observations obtained at the European Southern Observatory, La Silla, Chile, at the Cerro Tololo International Observatory, Chile, at the Las Campanas Observatory, Chile, at the German-Spanish Calar Alto Observatory, Spain, and at the La Palma Observatory, Spain.

were directed toward the measurement of spectroscopic velocities,  $v \sin i$ , which are now known for more than 130 TTS, thus providing a large enough database to investigate the rotational properties of these stars on a statistical basis (Vogel & Kuhi 1981; Bouvier et al. 1986b; Hartmann et al. 1986; Hartmann & Stauffer 1989; Bouvier 1990; Bouvier 1991). The main results of these studies are the following. 1) Low-mass TTS have rotational velocities in the range from less than 10 up to 30 km s<sup>-1</sup>, with a mean rotational velocity of about 15 km s<sup>-1</sup>. Since protostars are expected to form with a velocity near break-up, large angular momentum loss must occur before the stars become visible. 2) The average rotational velocity increases with mass from about 15 km s<sup>-1</sup> at 1 M<sub>⊙</sub> to 40 km s<sup>-1</sup> at 2.0 M<sub>⊙</sub> and up to more than 100 km s<sup>-1</sup> for Herbig Ae-Be stars that are the more massive counterparts of the TTS. It is still unclear whether this mass-dependence reflects the initial angular momentum distribution of stars as they form or whether it results from the faster evolution of more massive stars on their radiative tracks. 3) Classical TTS (CTTS), which drive energetic winds and accrete from a circumstellar disk, have a rotational velocity distribution statistically similar to that of weak-line TTS (WTTS) which lack both strong winds and accretion disks. As Hartmann & Stauffer (1989) pointed out, the typical accretion rate of CTTS is estimated to be 10<sup>-7</sup> M<sub>⊙</sub> yr<sup>-1</sup> and this should lead to an acceleration of the central star up to a fraction of the break-up velocity on a timescale of a few 10<sup>6</sup> yrs if the circumstellar material is directly accreted onto the stellar equator. Since CTTS have a  $v \sin i$  amounting to only one tenth of the break-up velocity, the need for angular momentum loss was identified and their energetic winds were proposed as the most likely mechanism for angular momentum removal. More recent models suggest that accretion of circumstellar material on the stellar surface may actually lead to stellar spin-down rather than spin-up if the star is magnetically coupled to the inner regions of the circumstellar disk (Königl 1991; Camenzind 1990).

Although  $v \sin i$  studies have proven very useful in determining the statistical rotational properties of young stars, they suffer two major limitations. First,  $v \sin i$  measurements can only be used in a statistical way because of the unknown geometric effect included in  $\sin i$ . Second, the spectral resolution required to measure  $v \sin i$  less than 10 km s<sup>-1</sup> cannot usually be attained with current detectors for such faint stars as TTS, so that a number of TTS lack an accurate determination of their  $v \sin i$ , having only an upper limit of 10 km s<sup>-1</sup>. Because of these uncertainties, it is difficult to estimate the dispersion of angular momentum at a given age and mass from  $v \sin i$  distributions, and the actual distribution of rotation among slow rotators with  $v \sin i \leq 10$  km s<sup>-1</sup> is still unknown.

A more useful, but more difficult to obtain, measurement of rotation is the direct determination of the stellar rotational period. TTS are known to exhibit periodic light variations that are interpreted as resulting from the rotational modulation of the stellar flux by surface spots (e.g. Rydgren & Vrba 1983; Bouvier et al. 1986a; Vrba et al. 1986; Bouvier & Bertout 1989; Vrba et al. 1989). Therefore, the photometric period is a direct estimate of the star's rotational period which is not affected

by geometric effects and is usually derived with an accuracy of better than 10%. Rotational periods ranging from 1.5 to 8.5 days have been measured so far for 30 TTS (see a compilation by Bouvier 1991). Most of the photometric modulation studies, however, have been limited to the monitoring of TTS light curves on a time interval of 2 weeks, so that only rotational periods shorter than 10 days could be detected. As a result, the current rotational period distribution of TTS is biased towards the detection of relatively rapid rotators (Bouvier 1991).

In an effort to eliminate this bias and to determine the actual distribution of rotational periods among TTS, we started a long-term photometric monitoring campaign of a sample of TTS. The results of the first COYOTES campaign, an acronym for Coordinated Observations of Young Objects from Earthbound Sites, are presented in this paper. This campaign took place between November 1990 and February 1991 and was aimed at monitoring the light variations of 24 PMS stars. The observations were performed from 5 observatories and are described in an accompanying paper (Bouvier et al. 1993) where the photometric measurements as well as the mean UBVRI magnitudes of the sample stars are tabulated.

This first COYOTES campaign was aimed at answering the following questions. 1) What is the dominant source of photometric variability for TTS on a timescale of a few weeks? 2) What are the properties of the spots responsible for the rotational modulation of the stellar flux? 3) What are the rotation rates of PMS stars with a  $v \sin i$  less than 10 km s<sup>-1</sup>? Are these stars intrinsically slow rotators or merely moderate rotators seen at low axial inclination? 4) What is the total range of rotational periods exhibited by TTS? Bouvier et al. (1986b) found no stars with a  $v \sin i$  less than 6.7 km s<sup>-1</sup> in a sample of 21 TTS, which would correspond to a maximum rotational period of 14 days, assuming a stellar radius of 2 R<sub>⊙</sub>. 5) What is the dispersion of angular momentum among PMS stars of a given age and mass? As noted above, the angular momentum dispersion is difficult to estimate from  $v \sin i$  distributions because of the unknown  $\sin i$ . 6) Are the distributions of rotational periods the same for accreting and non-accreting young stars? And, more precisely, what is the effect of mass-accretion and mass-loss onto the rotational evolution of young stars?

In Sect. 2, the light curves obtained for 24 stars during the COYOTES campaign are presented and analyzed to search for a periodic component. The period search algorithms are briefly described and the model used to derive the properties of the spots responsible for the modulation of the stellar flux is discussed. Section 3 attempts to answer the questions listed above. It includes a brief description of the derived spots properties and a discussion of the rotational properties of T Tauri stars. We find in particular that WTTS rotate faster than CTTS, which suggests a different rotational evolution for stars of each subclass on their convective tracks. We explore the implications of this result for the subsequent rotational evolution of young stars towards the main sequence. The results are summarized in Sect. 4 and major remaining issues are outlined.

## 2. Results

UBVRI light curves were obtained for 13 classical T Tauri stars (DE Tau, DF Tau, DG Tau, DI Tau, DK Tau, DR Tau, GG Tau, GK Tau, IP Tau, RY Tau, GM Aur, SU Aur, LkCa-15), 10 weak-line T Tauri stars (IW Tau, LkCa-4, LkCa-7, LkCa-19, LkCa-21, TAP 9, TAP 26, TAP 40, TAP 41, TAP 57NW), and 1 suspected Herbig Ae star (BD +24°676). Their photometric variations were monitored over a period of 60 days, though adverse weather conditions resulted in large gaps in the light curve sampling. Further observations were obtained in February 1991 for 3 program stars (BD +24°676, DF Tau, RY Tau), resulting in a total time coverage of 90 days. The observational procedure and data reduction process are described in Bouvier et al. (1993, Paper I) where all the photometric measurements are tabulated.

### 2.1. Period analysis

The light curves obtained during the COYOTES campaign were first analyzed to search for a periodic component in the light variations. Two methods were used: the string-length method (Dworetsky 1983) and the periodogram analysis (Horne & Baliunas 1986). Periods were searched for within an interval ranging from  $P_{min}=2$  days to  $P_{max}=30$  days, the lower boundary corresponding to the generalized Nyquist frequency, i.e., twice the minimum sampling step, and the higher one to half the total observing period. In the string-length method, this interval is divided in 1000 steps ( $\delta P=0.028$  days) and a phase diagram is computed at each step, i.e., for each  $P_n=P_{min}+n \times \delta P$ . The “string-length” is defined as the sum of the distances between successive points in the phased light curve, and is computed for each  $P_n$ . The most likely period is then the  $P_n$  for which the minimum string-length is found.

The other method consists in computing the periodogram of the light curve, which is the discrete approximation to the Fourier transform of the data string. Unlike the string-length method, which does not assume any particular shape for the light curve, the Fourier analysis tries to reproduce the light curve in terms of sums of sinusoids. The periodogram is computed at 1000 frequencies between  $2\pi/P_{max}$  and  $2\pi/P_{min}$ , as defined above. The most likely period is indicated by the peak which has the highest power in the periodogram. For evenly sampled data, Horne & Baliunas (1986) provide an empirical rule that allows one to compute the significance level of a peak of a given height in the periodogram. This rule cannot be applied here due to the strongly uneven sampling of the COYOTES light curves. In order to assess the level of significance of the periodogram peaks, we therefore generated 3000 synthetic light curves consisting of normally-distributed random noise and having the same temporal sampling as the COYOTES light curves. We then selected the highest peak in each of the 3000 resulting periodograms and built the probability distribution. This distribution indicates the probability that a peak of a given height may occur by chance in the periodogram. We thus derived the minimum power that a peak must have in order to indicate a real period in the data at the 90%, 99% and 99.9% confidence level. These levels are

displayed together with the periodograms in the following analysis.

When applied to the stars of our sample, the string-length method and the periodogram analysis yielded the same results to within a fraction of a day for all but one star (TAP 41, see Sect. 2.4.9). Therefore, only the results of the periodogram analysis are described below. All the 24 stars observed during the COYOTES campaign are found to exhibit periodic variations with periods ranging from 1.2 to 24 days. Of these, 7 are confirmations of previously suspected periods, and 17 are new period determinations. The results for individual objects are presented in Sects. 2.3 and 2.4.

### 2.2. The spot model

In all but 4 cases (BD +24°676, RY Tau, LkCa-21, and TAP 26), the periodic light variations are interpreted as being due to the modulation of the stellar flux by surface spots. In a previous paper (Bouvier et al. 1986a), we used a geometrical spot model in order to reproduce the observed light curves from the U- to the I-band and derive the properties of the spots responsible for the periodicity. In order to be tractable analytically, such a model requires the assumption that a single circular spot is present at the stellar surface. Most likely, however, the surface of TTS is covered by several spots or spot groups. The evidence for multiple spots comes from extensive photometric monitoring of TTS over several years (e.g. Vrba et al. 1988) and from the results of Doppler Imaging applied to the weak-line TTS V410 Tau (Joncour & Bertout 1993). Most often, TTS light modulation results in quasi-sinusoidal light curves. Such a light curve shape can be due to a single, high-latitude spot that remains partly visible during the whole rotational cycle. However, when the star is observed at high inclination, the spot is expected to disappear onto the hidden hemisphere, and this results in a flat maximum light level in the light curve. The paucity of light curves exhibiting such a feature suggests that the quasi-sinusoidal shape is most likely the result of the existence of several spots on the stellar surface. In such a case, the one-spot model will erroneously lead to a spot located at high latitudes which mimics a more even spot distribution on the stellar surface.

In order to avoid this bias, we adopt here a spot model which does not make any assumption on the number of spots on the stellar surface nor on their shape. The model assumes, however, that the spots all have the same temperature. The price to pay for this simplification is that we are not able to derive the location of the spots on the star and that we can only deduce a *lower limit* to the fraction of the stellar surface covered by spots. Vogt (1981), after Torres & Ferraz Mello (1973), showed that the total amplitude of the light variations produced by stellar spots can be written as:

$$\Delta m(\lambda) = -2.5 \log \frac{1 - [1 - Q(\lambda)] \cdot G_{max}(\lambda)}{1 - [1 - Q(\lambda)] \cdot G_{min}(\lambda)} \quad (1)$$

where  $Q(\lambda)$  is the wavelength-dependent flux ratio between the spots and the photosphere, and  $G_{max}$  (resp.,  $G_{min}$ ) is the *projected* area covered by spots normalized to the surface of the



stellar disk at maximum (resp., minimum) spots visibility.  $G_{min}$  and  $G_{max}$  are free parameters that depend upon wavelength through limb-darkening effects<sup>1</sup>. Assuming that the star and the spots can be described as blackbodies, and that the spots all have the same temperature,  $Q(\lambda)$  contains only one free parameter, the spots temperature, while the stellar temperature is a fixed parameter deduced from the star's spectral type. Equation 1 therefore contains 3 free parameters. However, because  $G_{max}$  and  $G_{min}$  are strongly coupled, a further simplification of the model is desirable to avoid multiple solutions.

Equation 1 can be rewritten as:

$$\Delta m(\lambda) = -2.5 \log[1 - (1 - Q(\lambda)) \cdot G_{eq}(\lambda)] \quad (2)$$

where

$$G_{eq} = \frac{G_{max} - G_{min}}{1 - (1 - Q(\lambda)) \cdot G_{min}} \quad (3)$$

It can be shown that  $G_{eq} \leq G_{max} \leq S_{spot}/S_{disk}$ . Thus,  $G_{eq}$  is a *lower limit* to the true surface coverage by spots. Spot models based on Equation 2 have often been used in the literature for TTS and other late-type stars. There has been some confusion, however, about the meaning of  $G_{eq}$  which has sometimes been interpreted as being either the actual spot coverage or an *upper* limit to it, while it really is a *lower* limit to the true fraction of the stellar disk covered by spots. Assuming blackbody distributions for the star and the spots, Eq. (2) contains only 2 free parameters: the spots temperature and  $G_{eq}$ . These two parameters are derived from the model by fitting the  $\Delta m$  from Eq. (2) to the observed amplitudes of variations from the U to the I-band. Note that, regardless of the spots temperature, be it higher or lower than the stellar effective temperature, the amplitudes of the light variations *always* decrease toward longer wavelengths. Hot spots however can be distinguished from cool spots from the rate at which the photometric amplitudes decrease with wavelength. More precisely, hot spots produce a steeper decrease of the amplitudes with wavelength than cool ones.

Equation (2) is valid for a single star only. Since several stars in our sample are known visual or spectroscopic binaries, we should mention the effect that a companion may have on the determination of the spots properties. Assuming that the companion is an unspotted star, Equation (2) becomes:

$$\Delta m(\lambda) = -2.5 \log\left[1 - \frac{(1 - Q(\lambda)) \cdot G_{eq}(\lambda)}{1 + \frac{L_2}{L_1}(\lambda)}\right] \quad (4)$$

where  $L_2/L_1$  is the wavelength-dependent luminosity ratio between the secondary and the primary at maximum light (Vogt 1981). The effect of the companion is best illustrated by the following example. Let's assume a K7 star ( $T_{eff}=4000K$ ) with a 3000K spot covering 15% of the stellar surface. Then, according to Eq.2, the amplitudes of photometric variations are 0.62, 0.59,

0.52, 0.43, and 0.36 mag in the UBVRI-bands, respectively. We now assume that this star has an unspotted M8 companion ( $T_{eff}=2500K$ ) whose luminosity is the same as that of the primary at  $0.55\mu m$ . For blackbody distributions, this results in a luminosity ratio between the primary and the secondary of 0.13, 0.37, 1.0, 1.7, 3.2 in the UBVRI-bands, respectively. Putting these values in Eq.4, the UBVRI amplitudes of the light variations become 0.53, 0.40, 0.23, 0.14, 0.08, respectively. Hence, the effect of a companion is to significantly reduce the amplitude of light variations; the larger the flux ratio between the secondary and the primary, the greater the reduction.

Conversely, if we inject the K7 star+ M8 companion amplitudes derived in the example above into the single star model (Eq.2), i.e., if we ignore the presence of a companion, we would deduce a spot temperature of 5350K (instead of 3000K) and a spot fractional coverage of 2% (instead of 15%). Neglecting the presence of a companion, as far as it significantly contributes to the total luminosity of the system, can thus have quite dramatic effects on the derived spots properties. The example above shows that an IR companion, which contributes more light to the system in the red than in the blue, will reduce the photometric amplitudes in such a way as to mimic the presence of hot spots on the stellar surface. Hence, modeling the amplitudes of light variations may be a way, albeit very indirect, to detect the presence of IR companions in stars where hot spots are not expected to exist, e.g., in weak-line TTS.

Another complication to the model arises for stars whose energy distribution strongly departs from that of a blackbody. This is the case in particular for very active T Tauri stars that have strong UV and blue excesses. The continuum flux excess over the photospheric energy distribution is measured by the veiling produced on the photospheric spectrum (see, e.g. Basri & Batalha 1990), the veiling being defined as:

$$r(\lambda) = \frac{F_{tot}(\lambda)}{F_{\star}(\lambda)} - 1 \quad (5)$$

where  $F_{tot}$  is the total flux observed at the wavelength  $\lambda$  and  $F_{\star}$  is the contribution from the stellar photosphere only. Taking the veiling into account in the spot model, Eq.2 becomes:

$$\Delta m(\lambda) = -2.5 \log\left[1 - \frac{(1 - Q(\lambda)) \cdot G_{eq}(\lambda)}{1 + r(\lambda)}\right] \quad (6)$$

Since the veiling arises from a source of continuum radiation independent of the photosphere, it has the same reduction effect than a stellar companion onto the amplitude of light variations. Moreover, the continuum excess is larger in the blue than in the red part of the visible spectrum, so that the reduction of the amplitudes will be larger at shorter wavelengths. Neglecting the effect of veiling in the spot modeling will consequently lead to a temperature estimate which is a lower limit to the actual spots temperature.

It is clear from the above discussion that the spots properties derived from the spot model are only first order approximations to the actual spots properties. This is particularly true for very active T Tauri stars, such as DG Tau, whose energy distribution strongly departs from that of a blackbody. Because veiling is

<sup>1</sup> As shown by Torres & Ferraz Mello,  $G(\lambda)$  can be written as  $G'/\pi$  ( $1-\mu(\lambda)/3$ ), where  $G'/\pi$  is the ratio of the projected spotted area to the stellar disk surface and  $\mu(\lambda)$  the limb-darkening coefficients. Note that, contrary to what is sometimes stated in the literature, 0°K spots do produce color variations in the light curve because of the limb-darkening effects.

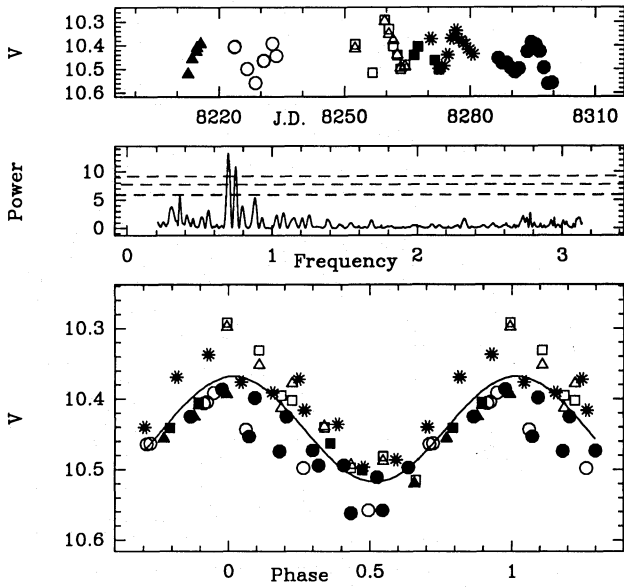


**Fig. 1.** BD 24°676. a) Direct V-band light curve. Symbols correspond to different observing runs: Calar Alto I (filled triangles), ESO (empty circles), La Palma (empty triangles and squares), Calar Alto II (filled squares), Las Campanas (stars), CTIO (filled circles). The abscissa is Julian Date - 2440000. b) Periodogram of the V-band light curve. The three dashed-lines correspond to probability levels of 90, 99, and 99.9%, respectively, that the periodogram peak corresponds to a real photometric period. The abscissa is angular frequency in  $\text{rad days}^{-1}$ , i.e.,  $2\pi/P$ . c) V-band light curve folded in phase with the most likely period (see text). A least-square sinusoidal fit is superimposed onto the phased light curve

known to be strongly variable on short timescales, simultaneous photometric and spectroscopic observations are required to properly include its effect in the spot modeling. An additional uncertainty on the spots properties arises for known binaries included in our sample: DF Tau, DI Tau, DK Tau, GG Tau, GK Tau, IW Tau, LkCa-7, TAP 9, and TAP 57NW (Simon et al. 1992; Leinert et al. 1992; Mathieu et al. 1989; Reipurth & Zinnecker 1992), though the extent to which the companion contributes to the total luminosity of these systems at optical wavelengths is usually unknown. For single, weak-line T Tauri stars, however, these complications do not occur, and the error on the spots temperature deduced from the model does not exceed 500K, while the relative uncertainty on the fractional surface coverage by spots is of the order of 30%, and mainly depends upon the quality of the light curve sampling as well as upon photometric measurement errors.

### 2.3. Classical T Tauri stars and Herbig Ae/Be stars

Periods and spots properties derived from light curves of classical T Tauri stars ( $\text{EW}(\text{H}\alpha) \geq 10\text{\AA}$ ) and of the suspected Herbig Ae star BD +24°676 are presented in this section. The star's most common name is used and the object's number in Herbig & Bell's (1988) catalogue is given, so that alternative names can be found there. For the spot model, the stellar effective temper-

ature was deduced from the spectral type using Cohen & Kuhn's (1979)  $\text{Sp-T}_{\text{eff}}$  scale, and the UBVRI limb-darkening coefficients for the relevant  $T_{\text{eff}}$  were interpolated from Al-Naimy's (1978) tables.

For each object, a four-panel figure displays: a) the observed light curve in the V-band; b) the corresponding periodogram; c) the V-band light curve folded in phase with the derived photometric period as well as a least-square sinusoidal fit to the phased light curve; and d) the amplitude of the light variations at several wavelengths together with the best fit obtained from the spot model. Since light curves at other wavelengths are very similar to the V-band light curve, only the latter is shown.

The results are summarized in Tables 1 and 2 for both CTTS and WTTS. The entries in Table 2 are as follow:

Column 1: star's name.

Column 2: rotational period in days.

Column 3: stellar effective temperature.

Column 4: spots temperature.

Column 5: fraction of the total stellar surface covered by spots ( $=G'/2\pi$ , see footnote 1). As explained above, this is a lower limit to the actual spot coverage.

#### 2.3.1. BD +24°676

BD +24°676 has recently been identified as a bright PMS star of the Taurus association by Weaver & Hobson (1988) on the basis of strong  $\text{H}\alpha$  emission ( $\text{EW}(\text{H}\alpha) = 10\text{--}15\text{\AA}$ ). A spectrophotometric study of this object led Walter et al. (1990) to classify BD +24°676 as a Herbig A3e star.

BD +24°676 is one of the stars for which we obtained extended time coverage leading to the 90-day light curve shown in Fig. 1a. The photometric variability reaches a total amplitude of 0.3 mag in the V-band on a time scale of a few weeks. This level of variability is typical of T Tauri stars but somewhat surprising for a Herbig Ae star. Herbst et al. (1982) found that none of the 7 Herbig Ae/Be stars they monitored displayed light variations above the 0.05 mag level.

The periodogram of BD +24°676's V-band light curve is shown in Fig. 1b and exhibits a major peak at a period of 9.0 days and a somewhat smaller peak at a period of 8.4 days. Only the 9.0-day peak is seen above the 99.9% confidence level simultaneously in the BVRI periodograms. The string-length method suggests a most likely period of 8.8 days in all photometric bands. We thus conclude that BD +24°676's light curve exhibits a periodicity of  $8.8 \pm 0.2$  days. The phased light curve is shown in Fig. 1c and bears marginal evidence for a slight change of maximum brightness level during the observing period.

Unlike all the other stars in our sample, BD +24°676 gets bluer when fainter. This color behavior cannot be reproduced by assuming the presence of hot or cool spots at the stellar surface, neither can it be due to circumstellar extinction. Instead, it suggests that BD +24°676 might be a spectroscopic binary, so that the 8.8d periodic wave may correspond to the orbital period of the system rather than to the rotational period of the star. In order to test this hypothesis, Martín (1992) obtained medium

resolution spectra of BD +24°676 and measured a radial velocity of  $+91 \pm 10$  km/s, quite inconsistent with Taurus membership.

Both the photometric behavior and the radial velocity of BD +24°676 cast doubt onto its PMS status. We therefore do not consider this star any further in the present study.

### 2.3.2. DE Tau (HBC 33)

DE Tau's light curve (Fig. 2a) exhibits photometric variations with an amplitude of 0.3 mag in the V-band on a timescale of one week. The only significant peak in the periodogram (Fig. 2b) corresponds to a period of 23.5d and is seen above the 90% confidence level only in the V and R bands. The V light curve folded in phase with a period of 23.5d is shown in Fig. 2c. The scatter is large around the sinusoidal fit and it appears that the suspected period is mainly driven by a few ESO measurements near  $\Phi=0.5$  when the star was significantly fainter than during the rest of the observing period (see Fig. 2a). We therefore believe that this period is spurious and merely reflects non-periodic luminosity variations on a time-scale of a few weeks.

Since the light curve exhibits a constant average light level during the whole observing period except for the ESO run, we computed a new periodogram after having discarded ESO observations. The resulting light curve is shown in Fig. 3a and the corresponding periodogram in Fig. 3b. The UBVRI periodograms are dominated by a series of peaks that appear above the 90% level and correspond to a period interval ranging from 5.8 to 8.8d (Fig. 3b). Only one peak however is simultaneously seen in 4 bands (B, V, R, and I) above the 90% confidence level and suggests a period of 7.6d. The phased light curve in the V-band (Fig. 3c) is well reproduced by a sine wave but it also shows that the derived period is mainly driven by the La Palma run. For this reason, and because the ESO measurements do not fit into this result, we regard the 7.6d period for DE Tau as tentative rather than conclusive.

The amplitudes of the light variations as a function of wavelength from U to I are shown in Fig. 3d. Assuming that the photometric variability is due to rotational modulation, these amplitudes are best reproduced by stellar spots that are hotter than the photosphere ( $T_{eff}=3680K$ ,  $T_{spot}=4770K$ ) and cover 1.3% of the stellar surface. DE Tau is known to exhibit moderate veiling ( $r \leq 1.0$ , Basri & Batalha 1990) which was not accounted for in the spot model, so that the derived spots temperature must be viewed as a lower limit to the actual spots temperature.

### 2.3.3. DF Tau (HBC 36)

DF Tau was included in the photometric campaign in order to investigate the 8.5 day period previously reported by Bouvier & Bertout (1989). The light curve obtained during the COYOTES campaign spans almost 90 days and is shown in Fig. 4a. When the whole light curve is analyzed, no peak occurs in the periodogram above the 90% confidence level in any color. Since the 8.5d period is known to be unstable (it was identified on a light curve obtained in 1984 but not seen later on two light curves obtained in 1986, see Bouvier & Bertout 1989), we re-

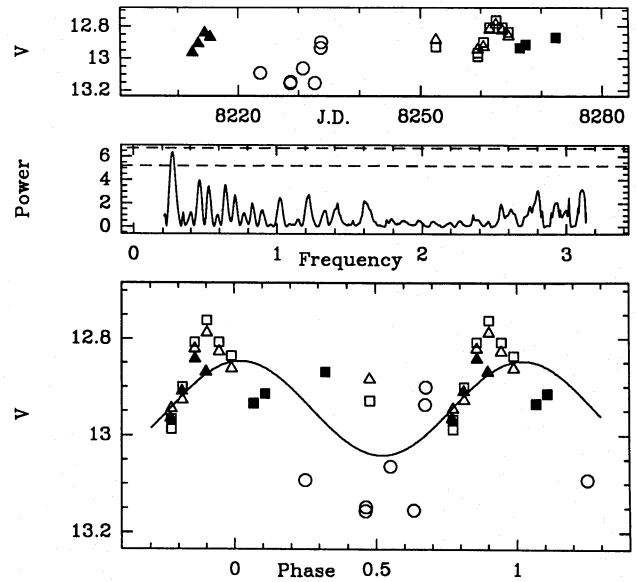


Fig. 2. DE Tau. Panels are as in Fig. 1

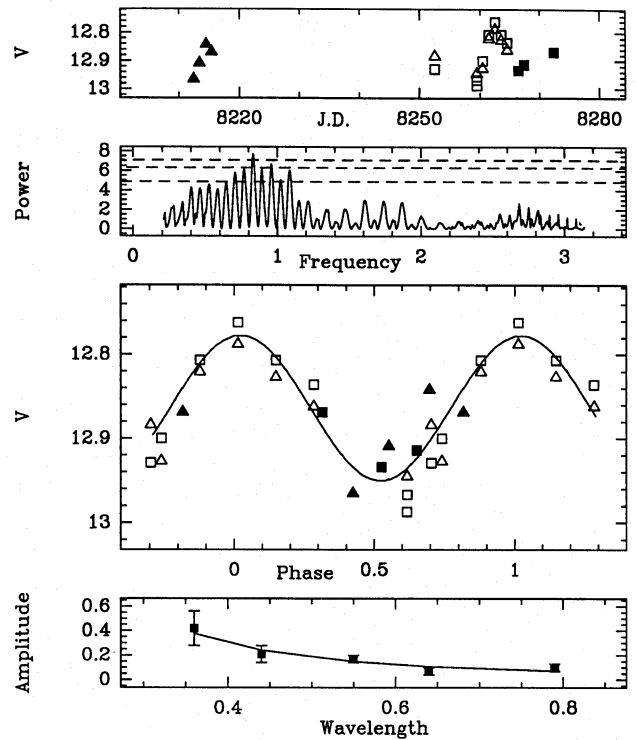


Fig. 3. DE Tau. Panels a), b), c) are as in Fig. 2 except that ESO data have been discarded (see text). Panel d) shows the total amplitude of the light variations as a function of wavelength in the UBVRI bands and the solid line illustrates the best spot model (see text)



summed the periodogram analysis on only part of the light curve. Because the full moon was crossing over Taurus during part of the ESO run, thus leading to measurements of lower quality for such a faint star as DF Tau, we first removed the ESO data from the light curve. The periodogram of the remaining light curve exhibits a 8.5d period peak in the UBV bands above the 90% confidence level (Fig. 4b). No other peaks with a similar power are simultaneously seen in several colors. The COYOTES light curve thus supports the previously reported 8.5d period for DF Tau. The phased light curve is shown in Fig. 4c and reveals a large degree of irregular variability superimposed upon the periodic variations.

The amplitudes of variations as a function of wavelength (Fig. 4d) are significantly lower than those observed in the 1984's light curve (see Bouvier & Bertout 1989). The best spot model indicates a spot temperature of 5140K ( $T_{eff}=3800K$ ) and a fractional surface coverage of 3%, but the resulting fit only marginally agrees with the observations ( $\chi^2=5.3$ , See Fig. 4d). This probably results from the fact that we neglected both the effect of veiling on DF Tau's energy distribution ( $r \approx 1.0$ , Basri & Batalha 1990) and the presence of a near-IR companion detected by Chen et al. (1990) from lunar occultation observations. The spot properties derived from the model are therefore uncertain. Nevertheless, the presence of a hot spot at the surface of DF Tau is independently supported by the simultaneous photometric and spectroscopic observations of Walker (1987) who finds that the depth or intensity of absorption and emission lines, respectively, decreases when the star gets brighter. He argues that this behavior results from the contribution of a source of continuous emission separate from the photosphere or the chromosphere, which is consistent with Bertout et al.'s (1988) hypothesis that a hot spot, which would result from the accretion shock near the stellar surface, is responsible for DF Tau's periodic light variations.

Moreover, we performed simulations to check whether the remarkable amplitudes of the light variations observed in DF Tau's 1984 light curve could be reproduced by cool spots when accounting for the presence of the companion. A solution was found for 1500K spots covering 30% of the stellar surface and for a luminosity ratio between the secondary and the primary of 0.0, 0.3, 0.9, 1.7, and 3.0 in the UBVRI bands, respectively. This would imply that the companion is much brighter than DF Tau in the near-IR, which is contrary to the results of Chen et al. (1990) who find that the primary is brighter than the secondary by a factor of 1.4 at  $2.2\mu m$ . We therefore conclude that the evidence for hot spots at the surface of DF Tau is robust.

#### 2.3.4. DG Tau (HBC 37)

DG Tau is an extreme T Tauri star whose photospheric spectrum is completely veiled by continuous emission. While this star is known to exhibit strong flare-like activity, it was included in our sample with the hope that extended monitoring would allow us to disentangle rotational modulation from irregular variability. The V light curve obtained during the COYOTES campaign is shown in Fig. 5a and the V-band periodogram in Fig. 5b. A single

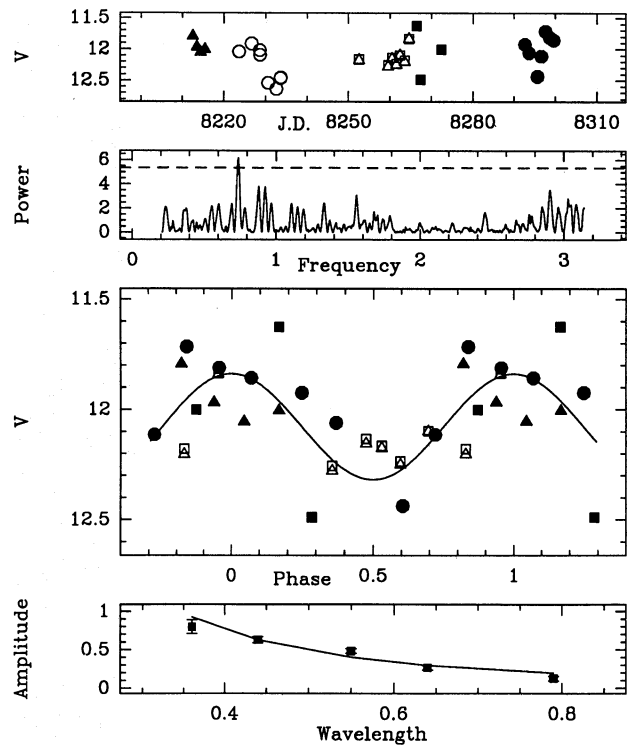


**Fig. 4.** DF Tau. Panels a), b), c) are as in Fig. 1. Panel d) shows the total amplitude of variation as a function of wavelength in the UBVRI bands and the solid line corresponds to the best spot model. ESO data have been discarded in panels b), c), and d) (see text)

peak corresponding to a period of 6.3d dominates the V-band periodogram and is also seen in the other colors above the 99.9% confidence level, a result confirmed by the string-length method. The V-band light curve folded in phase with a period of 6.3d is shown in Fig. 5c and exhibits a relatively smooth photometric wave with an amplitude of 0.4 mag, which suggests that DG Tau was in a relatively quiescent phase of activity during our observations.

From simultaneous photometric and spectroscopic observations, Walker (1987) concludes that the light variations of DG Tau are due to an independent source of continuum emission, as in DF Tau. Yet, we find that the amplitudes of variations (Fig. 5d) are well reproduced by assuming the existence of spots slightly cooler than the photosphere ( $T_{spot}=3430K$ ,  $T_{eff}=3920K$ ) covering 15% of the stellar surface. As discussed in Sect. 3.2, the spot model tends to underestimate the spot temperature when the spectral energy distribution of the star is significantly affected by veiling, as in DG Tau's case. In order to quantify this effect we recomputed the best fit to the amplitudes taking into account a wavelength-dependent veiling of 4.0 at U, 3.0 at B, 2.0 at V, 1.8 at R, and 1.5 at I, as estimated from Fig. 3 of Basri & Batalha (1990). We then find a spot temperature of 4850K and a fractional spot coverage of 15%. The corresponding fit to the amplitude of the light variations is shown in Fig. 5d as a dashed line and is nearly indistinguishable from the cool spot, no veiling solution.

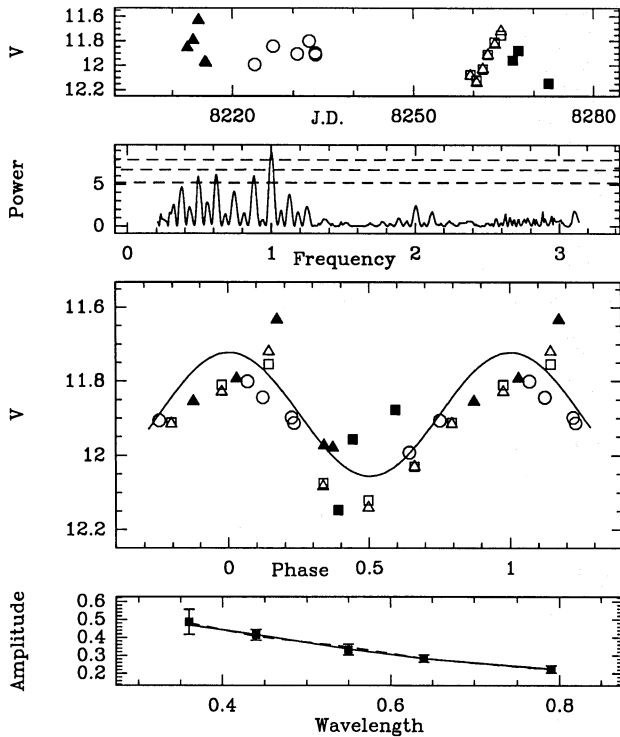


**Fig. 5.** DG Tau. Panels are as in Fig. 4. The dashed line in panel d) shows the best fit to the observations taking veiling into account in the spot model (see text)

### 2.3.5. DI Tau (HBC 39)

With an  $H_{\alpha}$  equivalent width of  $2\text{\AA}$  and a negligible near-IR excess (Strom et al. 1989a), DI Tau has the spectral characteristics of a WTTS. Yet, it was first detected together with a number of CTTS during an  $H_{\alpha}$  prism-objective survey of the Taurus cloud by Joy (1949). As Herbig & Bell (1988) pointed out, owing to the low detection limit of such a survey, DI Tau must then have had a much larger  $H_{\alpha}$  equivalent width than today. We therefore consider this star as being a CTTS which is apparently experiencing a quiescent phase of activity. From lunar occultation observations, Chen et al. (1990) discovered the existence of a companion 8 times fainter than DI Tau in the K-band at a projected separation of 72 mas.

Vrba et al. (1989) reported a photometric period of 7.9d with an amplitude of 0.02 mag for DI Tau. The light curve obtained during the COYOTES campaign (Fig. 6a) reveals a somewhat larger level of photometric variability with a total amplitude of 0.1 mag in the V-band. The periodogram analysis was performed on the VRI light curves only since the faintness of the star leads to unreliable measurements in the U and B bands. The V and R periodograms exhibit a single peak above the 99.9% confidence level at a period of 7.5d (Fig. 6b), consistent with Vrba et al.'s result. The V-band light curve folded in phase with a 7.5d period is shown in Fig. 6c. Lacking reliable U and B light curves, we are unable to derive the properties of the spots responsible for the light modulation.

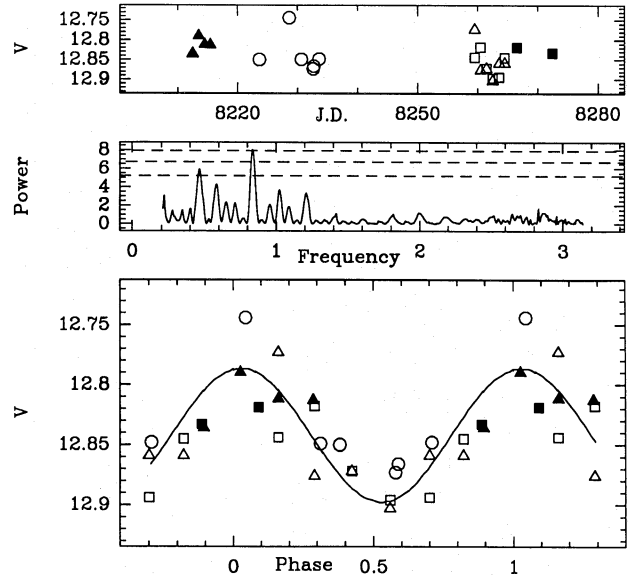


**Fig. 6.** DI Tau. Panels are as in Fig. 1

### 2.3.6. DK Tau (HBC 45)

The photometric variations of DK Tau were monitored by Rydgren et al. (1984) during 14 nights. Although the star exhibited significant light variations with an amplitude of nearly 1 mag in the V-band, the light curve did not reveal any evidence for periodicity at that time. Shevchenko et al. (1991), however, report a very significant period of 8.2d for DK Tau based on the analysis of the star's light variations from 1987 to 1990.

DK Tau's V-band light curve (Fig. 7a) obtained during the COYOTES campaign exhibits a constant mean light level except during ESO observations where the star was slightly brighter. As for DE Tau (see above), this is the reason why the periodogram of the raw light curve exhibits a relatively strong peak at a period of 25 days (Fig. 7b). However, there is an even stronger peak in the periodogram corresponding to a period of 8.37d. This peak is seen above the 99% confidence level in all the photometric bands. It is associated with a secondary peak at a period of 7.22d that reaches the 90% confidence level in the B, V, and R periodograms. These two peaks still dominate the periodograms at a confidence level greater than 99% in all bands when ESO measurements are discarded while the 25d period peak is then reduced well below the 90% confidence level.

In order to check whether the 7.22d and 8.37 periods are aliases, we constructed a synthetic light curve consisting of a pure 8.37d period sinusoid with the same temporal sampling as DK Tau's light curve. The periodogram exhibits both the 8.37d peak and the 7.22d alias peak, which confirms that the true photometric period of DK Tau is 8.37d, consistent with Shevchenko et al.'s (1991) result. The V-band phased light curve is shown in Fig. 7c and exhibits a large scatter around the mean sine wave, especially near minimum brightness. A similar scatter is apparent in Shevchenko et al.'s (1991) light curve and indicates strong irregular variability superimposed upon the rotational modulation.



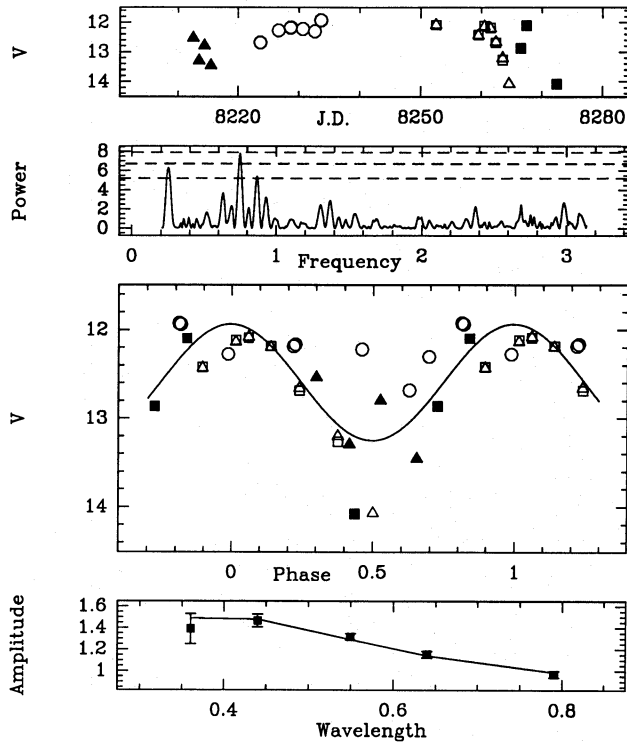


Fig. 7. DK Tau. Panels are as in Fig. 4

The slowly decreasing amplitudes of light variations towards longer wavelengths (Fig. 7d) are well reproduced by assuming that the modulation results from dark spots ( $T_{\text{spot}}=2410\text{K}$ ,  $T_{\text{eff}}=4000\text{K}$ ) that cover 25% of the stellar surface. This is one of the largest spot group detected so far on a T Tauri star (see Bouvier & Bertout 1989). Note that this result neglects both the influence of veiling which, however, is small in this star ( $r \approx 0.5$ , Basri & Batalha 1990) and the existence of a companion  $2.5''$  away from DK Tau (Reipurth & Zinnecker 1992).

### 2.3.7. DR Tau (HBC 74)

Like DG Tau, DR Tau is an extreme T Tauri star whose photospheric spectrum is completely veiled by continuous emission. The V light curve is shown in Fig. 8a and displays light variations with an amplitude of 1 mag while the mean light level remained nearly constant over the whole observing period. The periodogram analysis (Fig. 8b) reveals two peaks at or above the 90% confidence level in all colors: one at a period of 2.8 days, the other at a period of 7.3 days, the former being higher than the latter in all colors but U. Similarly, the string-length method suggests that the 2.8d period is more likely than the 7.3d period. In order to check whether these two periods are aliases, we constructed two sinusoidal light curves with a period of 2.8 and 7.3 d, respectively, that have the same temporal sampling as DR Tau's light curve. The periodogram of the 2.8d sinusoidal light curve does not show an alias peak at 7.3d, nor does the 7.3d light curve at the 2.8d period. This result indicates that the

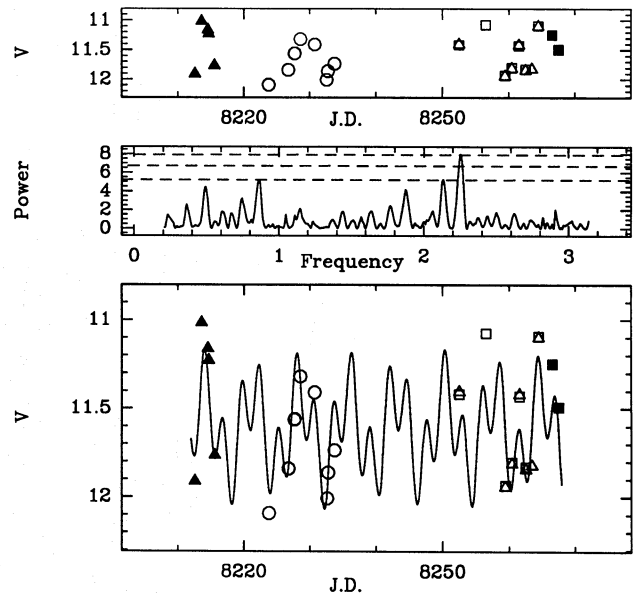


Fig. 8. DR Tau. Panels a) and b) are as in Fig. 1. Panel c) shows the direct light curve fitted by the sum of two sinusoids with periods of 2.8 and 7.3 d (see text)

two periods are indeed present in the light curve and not merely aliases.

Because of the presence of two periods in the data, we cannot show a phased light curve. Instead, Fig. 8c shows DR Tau's direct light curve to which the sum of two sinusoids with periods of 2.8 and 7.3 d was fitted. We cannot ascribe unambiguously one of these two periods to rotational modulation since both are consistent with the  $v \sin i$  measured for this star ( $v \sin i \leq 10 \text{ km.s}^{-1}$ , Hartmann & Stauffer 1989). Consequently, we did not attempt to apply the spot model to the observed light variations. The existence of two periods in the light curve may indicate that DR Tau is in fact a binary system. Further photometric monitoring and simultaneous spectroscopy are required to clarify their origin.

### 2.3.8. GG Tau (HBC 54)

Vrba et al. (1989) monitored the light variations of GG Tau over a period of 2 weeks and reported a possible period of about 10 days in the V-band but questioned its reality on the ground that it was not observed at other wavelengths. GG Tau was included in our sample in order to check for the existence of this period. The V-band light curve obtained over more than 8 weeks during the COYOTES campaign is shown in Fig. 9a and the corresponding periodogram is displayed in Fig. 9b. A single peak appears above the 99.9% confidence level at a period of 10.3d in the V-band periodogram, and is seen with a similar power in the B, R, and I bands. Our observations thus confirm and refine the previously suspected period. GG Tau's V-band light curve folded in phase with  $P=10.3\text{d}$  is displayed in Fig. 9c.

The amplitude of the light variations are plotted as a function of wavelength from U to I in Fig. 9d. The best spot model

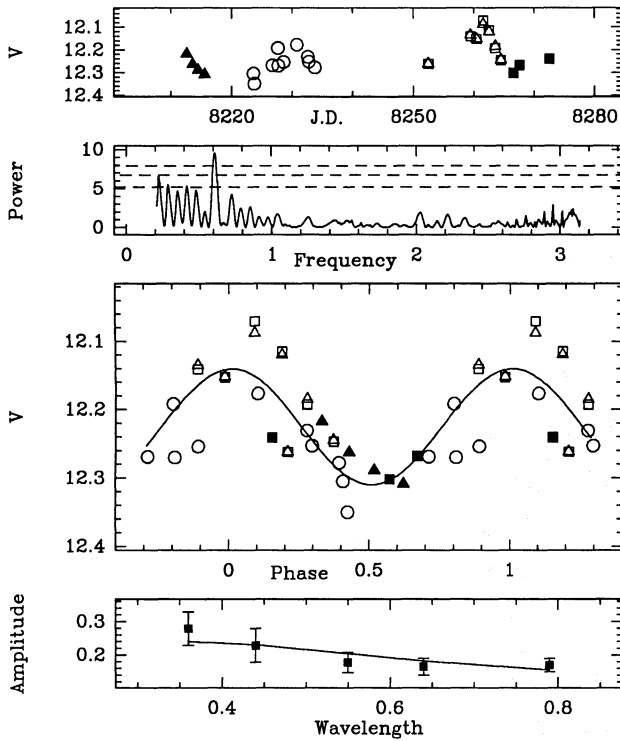


Fig. 9. GG Tau. Panels are as in Fig. 4

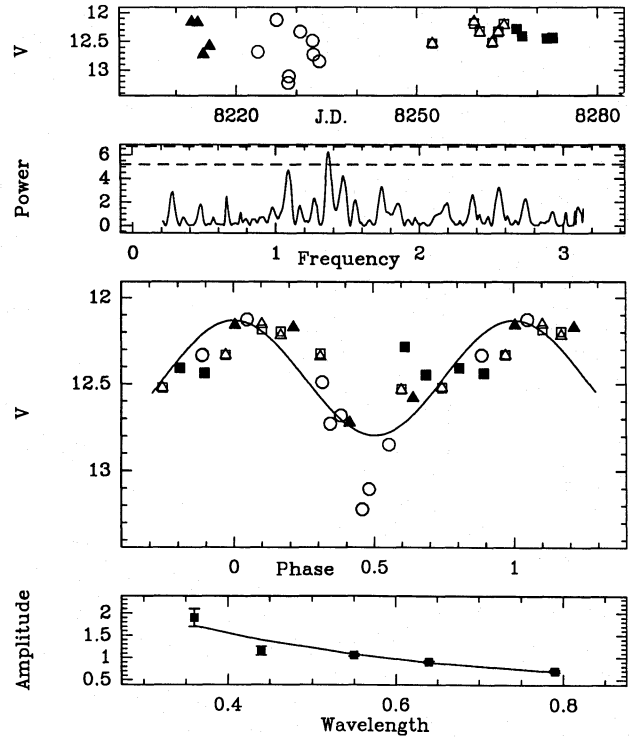


Fig. 10. GK Tau. Panels are as in Fig. 4

marginally agrees with the observations ( $\chi^2=0.7$ ) and indicates spots nearly 1000K cooler than the photosphere ( $T_{spot}=3030K$ ,  $T_{eff}=4000K$ ) that cover 7% of the stellar surface. While GG Tau exhibits small veiling at wavelengths larger than  $0.5\mu m$  ( $r \approx 0.5$ , Basri & Batalha 1990), its U and B colors may be more significantly affected ( $r \approx 1.5$ ). Since we did not account for veiling in the spot modeling, the derived spots temperature is to be regarded as a lower limit. Moreover, GG Tau is known to be a quadruple system (Leinert et al. 1991), which induces further uncertainty on the derived spots properties.

### 2.3.9. GK Tau (HBC 57)

Vrba et al. (1986) obtained two UBVRI light curves for GK Tau, each covering a period of 20 days and separated by 80 days. The first light curve is characterized by a series of non-periodic deep minima with an amplitude of 1 mag, while these minima are not seen in the second light curve. From a periodogram analysis of the light curves they deduced a likely period of  $4.6 \pm 0.1d$  for this star.

GK Tau's light curve was recorded over a period of 60 days during the COYOTES campaign (Fig. 10a). It exhibits the same range of variability than observed by Vrba et al., i.e., about 1 mag in the V-band, but the sampling is too loose to clearly identify the occurrence of successive deep minima. A single peak is seen simultaneously in 4 colors above the 90% level in the periodograms (Fig. 10b) and corresponds to a period of 4.65d. This period is also found to be the most likely in the B, V, R and I from the string-length method. This value is in excellent

agreement with Vrba et al.'s result and the V-band light curve folded in phase (Fig. 10c) suggests the existence of a narrow, deep minimum as they previously reported.

The variation of the full amplitude of the deep minimum as a function of wavelength is shown in Fig. 10d. The best fit indicates that the light modulation is due to spots hotter than the photosphere, with a temperature of 4810K ( $T_{eff}=4000K$ ), that cover 30% of the stellar surface. Such spots reproduce well the observations except in the B-band, where the observed amplitude is smaller than expected from the model. Vrba et al. (1986) derived similar spot properties ( $T_{spot}=4855K$ ,  $f/2=20.6\%$ ) from the deep minima they observed in GK Tau's light curve in 1983. Both studies neglect the presence of a companion located  $2.5''$  away from GK Tau (Reipurth & Zinnecker 1992). The flux ratio between the companion and GK Tau is only 0.03 at  $0.9\mu m$ , so that it is unlikely to strongly affect the results of the spot model.

### 2.3.10. IP Tau (LkCa-8, HBC 385)

With a  $10\text{\AA}$   $H_\alpha$  equivalent width, IP Tau lies at the border between weak-line and classical T Tauri stars. The latter classification appears to be more correct as Hartmann et al. (1987) reported the presence of an inverse P Cygni profile in the  $H_\alpha$  line and because this star is known to have a significant near-IR excess ( $\Delta K=0.31$ , Strom et al. 1989a). Herbig et al. (1986) measure a radial velocity of  $0 \pm 2 \text{ km s}^{-1}$ , while Hartmann et al. (1987) find  $V_r=14.5 \text{ km s}^{-1}$ . These discrepant results raise the possibility that IP Tau is a spectroscopic binary.

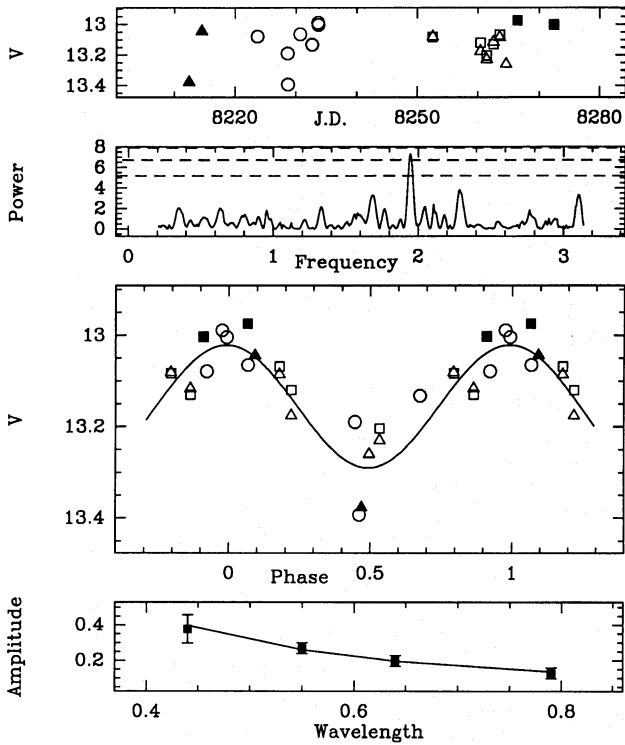


Fig. 11. IP Tau. Panels are as in Fig. 4

IP Tau's light curve in the V-band is displayed in Fig. 11a. A single peak appears above the 90% confidence level in the BVRI periodograms, indicating a period of 3.25d (Fig. 11b). Due to the faintness of the star in the U-band ( $\langle U \rangle = 15.2$ ), the U light curve is dominated by measurement errors and was not considered in the analysis. The phased light curve is shown in Fig. 11c and the amplitudes of the light variations in the B, V, R and I-bands are plotted in Fig. 11d. The latter are well reproduced by assuming the existence of spots 1000K hotter than the photosphere ( $T_{spot} = 4930K$ ,  $T_{eff} = 3920K$ ) and covering only 3% of the stellar surface.

### 2.3.11. RY Tau (HBC 34)

RY Tau has long been subject to extensive photometric monitoring. A light curve covering from 1965 to 1985 appears in Herbst (1986). The most remarkable feature is the brightening of this star in 1983, when its V magnitude decreased from 11.0 to 9.5 over a period of a few months. Several suspected periods have been reported for this star. Herbst et al. (1987) found a moderately strong peak at a period of 5.6d in the periodogram of a 200-day, V-band light curve of RY Tau obtained in 1985/86. Herbst & Koret (1988), however, failed to confirm this result. Herbst et al. (1987) also found a significant low-frequency peak in their periodogram corresponding to a period of 66 days. As they pointed out, such a long period cannot be due to rotational modulation owing to the large  $v \sin i$  measured for this star ( $v \sin i = 50 \text{ km s}^{-1}$ , Hartmann & Stauffer 1989).

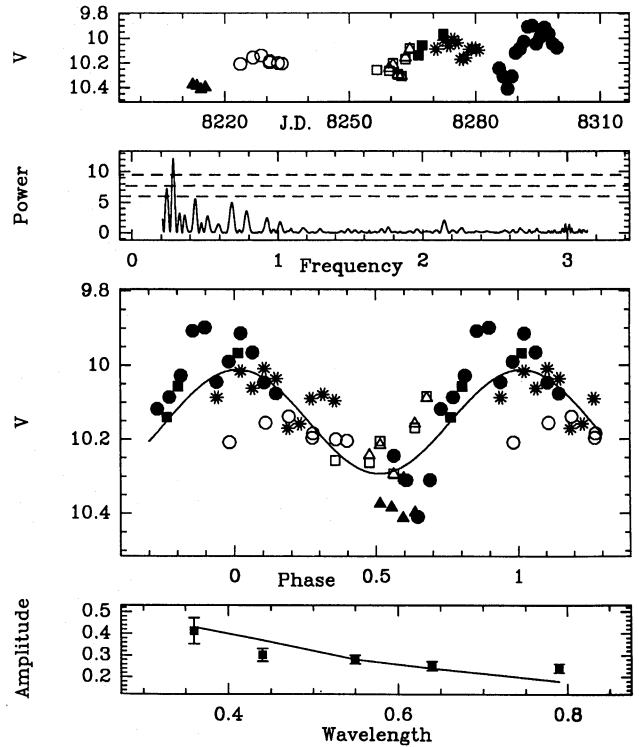


Fig. 12. RY Tau. Panels are as in Fig. 4. The solid line in panel d) shows the best fit to the observations assuming that the photometric variations are due to variable circumstellar extinction (see text)

RY Tau's light variations were recorded over almost 90 nights during the COYOTES campaign, with a night-to-night sampling during the last 40 nights. The resulting light curve in the V-band is shown in Fig. 12a. The range of variations, 9.8-10.4 in V, is similar to that regularly observed for this star since 1984. The periodogram (Fig. 12b) shows a peak at a period of 22.2d that reaches above the 99.9% confidence level in the 5 colors with an alias peak at a period of 26.4d. The string-length method suggests a most likely period of 24.7d in all colors. We conclude that, during our observations, RY Tau's light curve was periodic, with a period of  $24.0 \pm 2.0$  days. The phased light curve is displayed in Fig. 12c.

The previously reported 66d period cannot be searched for in our data because the light curve span too short a time interval. However, we are able to check the reality of the suspected 5.6d period, and do not find any evidence for its existence in any color. Conversely, we note that the second highest peak seen in the periodogram obtained by Herbst et al. (1987) corresponds to a period of about 24 days. Hence, although the 66 day period was dominating the light curve at that time, the 24 d period was very probably already present. We note that, given a 10% uncertainty in the period identification, the periods of Herbst and ours are close to harmonic or sub-harmonic multiples of one another:  $66/22=3$ ;  $22/5.6=4$ . Since the light curve appears non-sinusoidal, the 5.6d period may be a harmonic of the near-22d period.



Like the other T Tauri stars of this sample, RY Tau gets redder when fainter as expected from the modulation of the stellar flux by cool or hot spots. However, the observed photometric wave cannot result from rotational modulation since, for a measured  $v \sin i$  of  $50 \text{ km s}^{-1}$ , a rotational period of 24.0 days would imply a stellar radius of  $24 R_{\odot}$  or larger. The reddening of RY Tau as it becomes fainter is marginally consistent with the possibility that its photometric variations result from variable circumstellar extinction (Fig. 12d). This hypothesis, however, is not supported by Holtzman et al.'s (1986) simultaneous spectroscopic and photometric observations of RY Tau that show that the  $H_{\alpha}$  and  $H_{\beta}$  equivalent widths increase when the star gets fainter.

As a last resort, we mention the possibility that the 24.0d period may correspond to the orbital period of a binary system. In fact, RY Tau was once suspected to be a spectroscopic binary on the basis of radial velocity variations with a total amplitude of  $25 \text{ km s}^{-1}$  (Herbig 1977). However, more recent radial velocity measurements of higher accuracy suggest a constant radial velocity of  $16.5 \pm 2.4 \text{ km s}^{-1}$ , consistent with the velocity of the associated molecular gas (Hartmann et al. 1986). We also note that RY Tau has a flat IR energy distribution, which, in other similar objects, is attributed to the existence of an IR companion (e.g. T Tau –Ghez et al. 1991–, Haro 6-10 –Leinert & Haas 1989–, XZ Tau –Haas et al. 1990). Clearly, RY Tau is a complex object with two clearly identified photometric periods (24.0 and 66 days) which deserve further simultaneous photometric and spectroscopic studies.

### 2.3.12. GM Aur (HBC 77)

While the COYOTES campaign was in progress, we learned of a report by Kardopolov (1989) that GM Aur might be an eclipsing binary with an orbital period of 11.25 days. That GM Aur may indeed be a short period binary system is supported by the discrepant radial velocity measurements obtained for this star over the years (see Hartmann et al. 1986). We therefore added this star to our sample and obtained the light curve shown in Fig. 13a that spans a 40-day time period. Our data seems to confirm the existence of the previously reported period as the BVR periodograms do show a single peak above the 90% confidence level corresponding to a period of 12.0 days (Fig. 13b).

The UBVR light curves folded in phase with a period of 12.0d are shown in Fig. 14. The star exhibits quasi-sinusoidal light variations that are best seen in the B light curve. There are, however, a couple of points near the light minimum that strongly depart from the overall photometric wave. These two points are located at a phase of 0.31 and 0.40, respectively, and correspond to measurements obtained on two successive nights (J.D. 8285.6 and 8286.6, respectively). On the first night, the star had colors similar to those observed during the rest of the run but is 0.2 magnitude fainter than expected from the sinusoidal fit. This does not make much of a difference in the U and B bands since the total amplitude of the light variations is much larger but results in a large departure from the average light

curve in the V, R and I-bands. On the second night, the star appears very much redder than during the rest of the run with a I-magnitude close to the mean light level but with a U-magnitude almost 2 mag fainter than expected from the sine-curve fit. The origin of this sudden color change occurring close to minimum brightness is unclear but intriguing in the light of Kardopolov's (1989) claim that GM Aur may be an eclipsing system. Because it was a one-time occurrence during the whole run, we cannot dismiss the possibility that it is an artifact resulting from, e.g., the drift of the object in the diaphragm during the observing sequence. However, we find no indications in the observing logs that such a problem might have occurred. Certainly, this star deserves further photometric monitoring with a narrow temporal sampling.

At any rate, the periodograms still show a single peak at a period near 12 days above the 90% confidence level in all colors when these two data points are removed from the analysis. Therefore, the existence of this period is a robust result. The UBVR amplitudes of the quasi-sinusoidal light variations are shown in Fig. 13c. A good fit is obtained for spots with a temperature of  $5810 \text{ K}$  ( $T_{\text{eff}} = 4000 \text{ K}$ ) covering 0.7% of the stellar surface. We caution, however, that the presence of a companion, as far as it significantly contributes to the total luminosity of the system, may affect the accuracy of the spots temperature derived from the model.

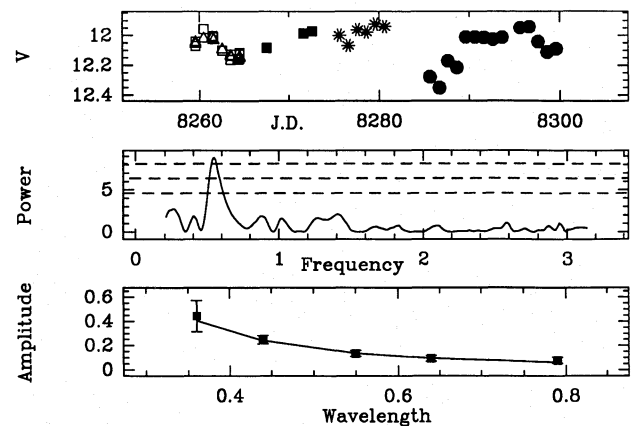


Fig. 13. GM Aur. Panels are as in Fig. 1

### 2.3.13. SU Aur (HBC 79)

SU Aur has sometimes been classified as a WTTS on the basis of its small  $H_{\alpha}$  equivalent width ( $EW(H_{\alpha}) = 4 \text{ \AA}$ ). Yet, the  $H_{\alpha}$  line flux is large and quite similar to that of other CTTS (Bouvier 1990a), which indicates that the small  $EW(H_{\alpha})$  merely results from a contrast effect against the bright stellar photosphere ( $Sp = G2$ ). Moreover, this star has a strong near-IR excess (Strom et al. 1989a) and we therefore conclude that it is a *bona fide* CTTS. SU Aur is one of the most rapidly rotating TTS measured so far with a  $v \sin i$  of  $65.0 \pm 3.5 \text{ km s}^{-1}$  (Hartmann & Stauffer 1989). It is therefore expected to have a short rotational

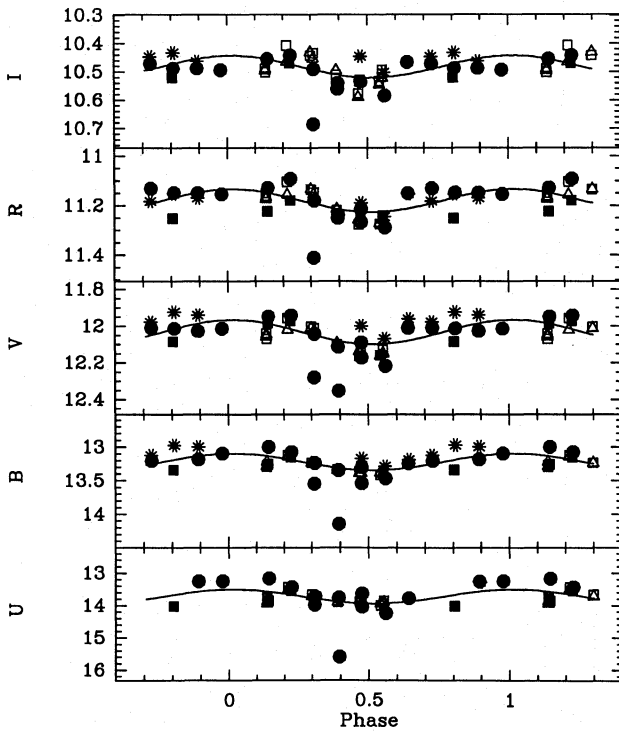


Fig. 14. UBVR light curves of GM Aur folded in phase with a period of 12.0d

period, of the order of 3 days or less for  $R_*=3R_\odot$ . Herbst et al. (1987) reported a possible period of 1.55 or 2.73 days for this star but were unable to confirm that result later on (Herbst & Koret 1988).

The light curve we obtained for SU Aur (Fig. 15a) exhibits a steady increase during the whole observing period. This linear trend was removed in each photometric band before the periodogram analysis was performed by setting the mean light level of each run to the same value. The resulting periodograms (Fig. 15b) exhibit 4 significant peaks above the 90% confidence level that are simultaneously seen in at least 3 colors. They correspond to periods of 1.47, 1.57, 2.78, and 3.37 days, two of which are similar to those reported by Herbst et al. (1987). All these periods are aliases, which makes difficult the determination of the true period. There is some indication that the most likely period is 2.78d since only the periodogram of a 2.78d sinusoid having the same temporal sampling as SU Aur's light curve exhibits alias peaks at the three other periods. Yet, the 2.78 d peak is not the dominant one in the periodogram of SU Aur's light curve. Because of these uncertainties, we conservatively conclude that the light variations of SU Aur are due to rotational modulation with a period shorter than 3.4 days. For illustration purpose, the V-band light curve folded in phase with a period of 2.78 days is displayed in Fig. 15c.

SU Aur is the earliest type star of our sample ( $Sp=G2$ ). It is also the star that has the lowest amplitudes of light variations, amounting to less than 0.1 mag at any wavelength (see Fig. 15d). This cannot be due to a projection effect, since SU Aur's large  $\sin i$  suggests that the star is seen at a relatively

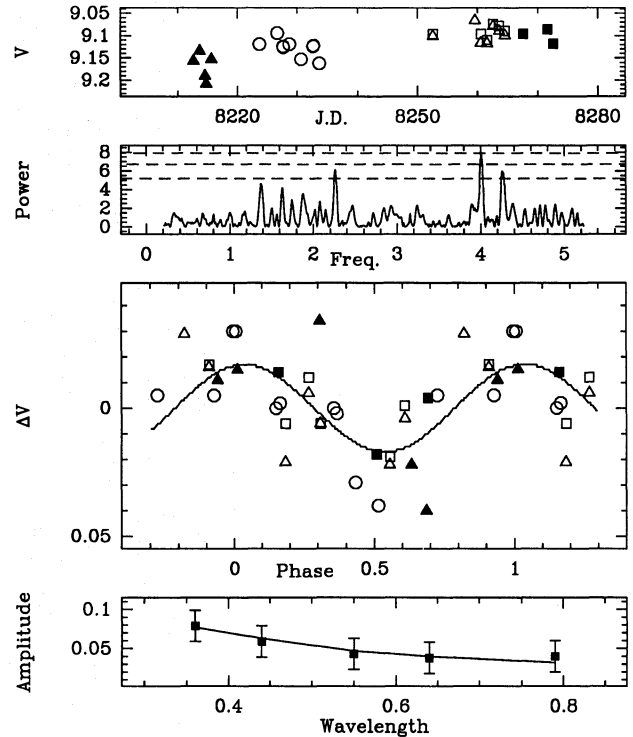


Fig. 15. SU Aur. Panels are as in Fig. 4. The periodogram and phased light curves were computed after setting the mean light level of each run to the same value (see text)

large inclination. The UBVR amplitudes are in fact well reproduced by assuming the existence of spots covering 21% of the stellar surface with a temperature of 5670K, i.e., only 100K cooler than the photosphere ( $T_{eff}=5770K$ ). This suggests that SU Aur's low-level variability results from a low contrast between the spots and the photosphere rather than from a small spot coverage.

#### 2.3.14. LkCa-15 (HBC 419)

A K5 star near the bottom of its Hayashi track in the H-R diagram, LkCa-15 was first detected in Herbig et al.'s (1986) CaII H and K survey of the Taurus cloud. They measure an  $H_\alpha$  equivalent width larger than  $29\text{\AA}$ , which must be a relatively recent occurrence since this star was not detected in previous  $H_\alpha$  surveys of the cloud. Hartmann et al. (1987) report an  $H_\alpha$  equivalent width of  $12.7\text{\AA}$ , which confirms that large variations of the  $H_\alpha$  line intensity may occur on a relatively short timescale. According to its present-day spectral characteristics, this star is a classical TTS.

The V-band light curve of LkCa-15 is shown in Fig. 16a. The periodograms (Fig. 16b) exhibit a peak above the 99% confidence level in all bands but I for a period of 5.86d. When folded in phase with this period (Fig. 16c), the light curve exhibits a large scatter at the (poorly-sampled) minimum light level ( $\Phi=0.5$ ). In order to test the reality of the suspected period, we removed the 4 La Palma measurements near  $\Phi=0.5$ , where the

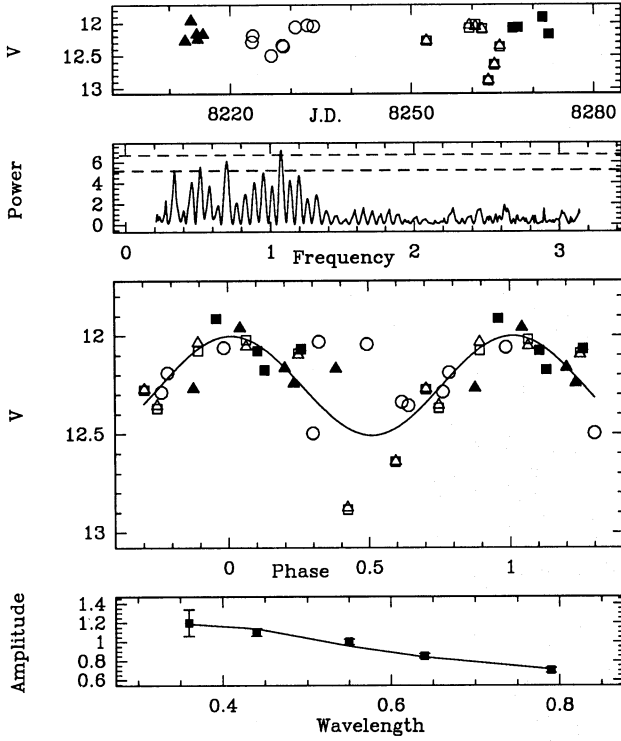


Fig. 16. LkCa-15. Panels are as in Fig. 4

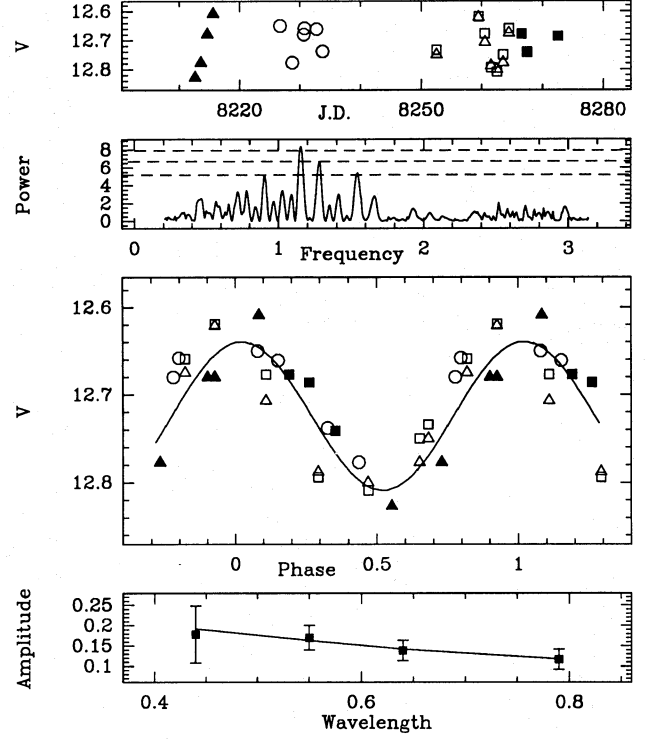


Fig. 17. IW Tau. Panels are as in Fig. 4

star was significantly fainter than during the rest of the observations, and recomputed the periodograms. It turns out that the 5.86d peak is still present but at a reduced level, reaching the 90% confidence level only in the U and B bands.

The total UBVR amplitudes of the light minimum seen in LkCa-15's light curve are shown in Fig. 16d. The best model solution corresponds to 3010K spots ( $T_{eff}=4395K$ ) with a fractional area of 22%.

#### 2.4. Weak-line T Tauri stars

We present in this section the photometric periods detected in the light curves of weak-line TTS (WTTS,  $EW(H_{\alpha}) < 10\text{\AA}$ ) together with the properties of the spots responsible for the rotational modulation of the stellar flux. The WTTS in our sample were selected from Herbig's et al. (1986) Ca II H and K survey of the Taurus-Auriga cloud (LkCa stars), and from Walter et al.'s (1988) spectrophotometric study of optical counterparts of X-ray sources detected by Feigelson et al. (1987, TAP stars).

##### 2.4.1. IW Tau (LkCa-16, HBC 420)

Discrepant radial velocity measurements were obtained by Herbig et al. (1986,  $V_{rad}=0\pm 4\text{ km s}^{-1}$ ) and by Hartmann et al. (1987,  $V_{rad}=15.8\pm 0.3\text{ km s}^{-1}$ ) for this  $1L_{\odot}$  K7 star. Leinert et al. (1992) report the presence of a companion at a distance of  $0.27''$  with a luminosity similar to that of IW Tau in the K-band. IW Tau's light curve in the V-band is plotted in Fig. 17a and the corresponding periodogram in Fig. 17b. A period of 5.45d

is present at or above the 99% confidence level in the BVR periodograms, while the string-length method suggests a most likely period of 5.6d. The light curve folded in phase with a period of 5.6d (Fig. 17c) shows quasi-sinusoidal variations with an amplitude of 0.2 mag in the V-band.

In Fig. 17d, the total amplitude of the minimum is plotted as a function of wavelength from B to I only since, with an average magnitude of 15.4 in the U-band, IW Tau's U-band light curve is dominated by measurement errors. The amplitudes are best reproduced assuming that cool spots ( $T_{spot}=3295K$ ,  $T_{eff}=4000K$ ) covering 7% of the stellar surface are responsible for the observed light variations. This solution does not take into account the presence of the companion whose contribution to the system's luminosity at optical wavelengths is unknown.

##### 2.4.2. LkCa-4 (HBC 370)

LkCa-4 is a relatively rapidly rotating ( $v\sin i=27\text{ km s}^{-1}$ , Hartmann et al. 1987), low-mass star ( $Sp=K7V$ , Herbig et al. 1986) located on the upper part of its Hayashi track in the H-R diagram. The V light curve covers a period of 60 days and is shown in Fig. 18a. Due to the faintness of the star in the U-band ( $<U=15.2$ ), measurements at this wavelength are not reliable and were not considered in the following analysis. The star exhibits night-to-night variability with an amplitude of 0.3 magnitudes in the V-band. The BVRI periodograms (Fig. 18b) are dominated by a single, very significant peak ( $\geq 99.9\%$  confidence level) indicating a period of 3.41d while the string-length method suggests a most likely period of 3.37d. The light curve folded in phase



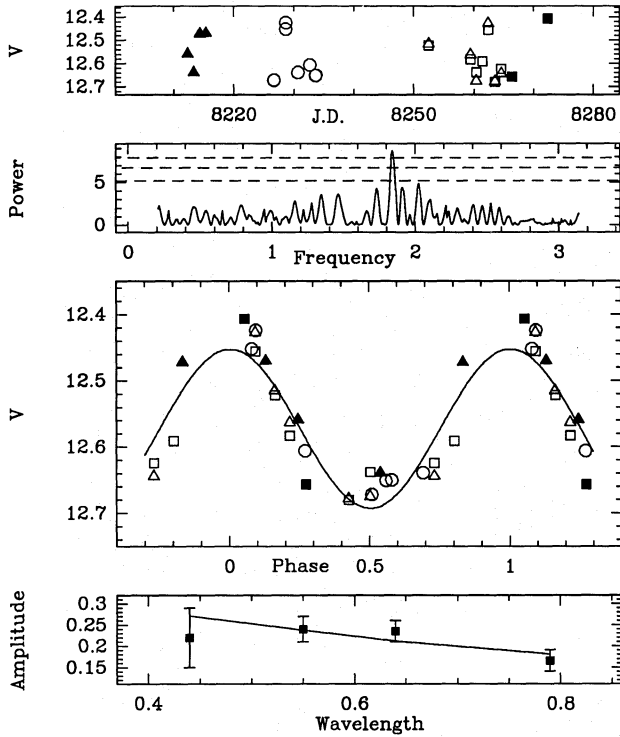


Fig. 18. LkCa-4. Panels are as in Fig. 4

with the latter period is shown in Fig. 18c. The best fit to the amplitudes of the light variations (Fig. 18d) is found for spots covering 8% of the stellar surface with a temperature of 3035K ( $T_{eff}=4000K$ ).

#### 2.4.3. LkCa-7 (HBC 379)

Close to LkCa-4 in the H-R diagram, LkCa-7 has also been detected as an X-ray source (041636+2743) by Walter et al. (1988). Leinert et al. (1992) report the presence of a companion at a distance of  $1.05''$  and a flux ratio of 0.56 in the K-band. The V light curve is shown in Fig. 19a and the corresponding periodogram in Fig. 19b. Both the periodogram analysis and the string-length method indicate a clear period of 5.64d in all colors with a confidence level larger than 99.9%. Vrba (priv. comm.) independently finds a period of 5.66d for this star, a preliminary report of which was given in Walter et al. (1992). The phased light curve (Fig. 19c) exhibits remarkably small scatter and reveals a broad, slightly asymmetric minimum. The total amplitude of the light minimum from U to I is best reproduced by spots much cooler than the photosphere ( $T_{spot}=2490K$ ,  $T_{eff}=4000K$ ) that cover 11% of the stellar surface (Fig. 19d). The fit is not very good, however, especially in the U-band, and the temperature estimate derived from the model may be affected by the unaccounted presence of LkCa-7's companion.

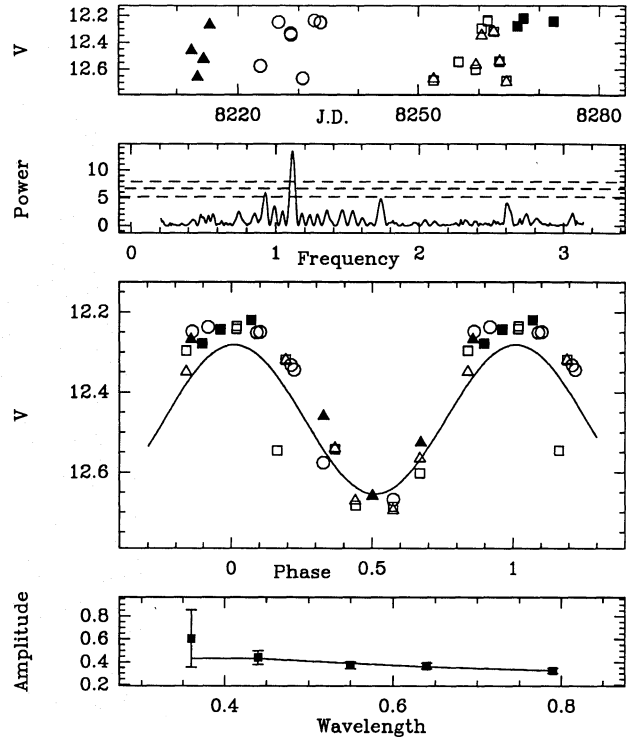


Fig. 19. LkCa-7. Panels are as in Fig. 4

#### 2.4.4. LkCa-19 (HBC 426)

A K0V star, LkCa-19 was independently detected in Herbig et al.'s (1986) CaII H and K survey and in Walter et al.'s (1988) X-ray survey of the Taurus-Auriga cloud. The V-band light curve (Fig. 20a) shows that the star undergoes rapid photometric variations from one night to the other with a total amplitude of 0.2 mag at this wavelength. The UBVRi periodograms all exhibit a peak above the 99% confidence level for a period of 2.24d together with an alias at a period of 2.13d (Fig. 20b) while the string-length method shows a deep minimum for a period of 2.24d, with no aliases. A V-band light curve folded in phase with a period of 2.24d (Fig. 20c) reveals quasi-sinusoidal light variations without any noticeable changes during the whole observing period. The amplitudes of the light variations from U to I are plotted in Fig. 20d, and best fitted by a model which indicates a temperature of 4770K for the spots ( $T_{eff}=5240K$ ) and a fractional spot coverage of 13%.

#### 2.4.5. LkCa-21 (HBC 382)

LkCa-21 was identified as a late-type ( $Sp=M3-4V$ ), weak-line TTS by Herbig et al. (1986). No photometry is reported by Herbig et al. for this star. During the COYOTES campaign, the star had  $\langle V \rangle = 13.5$  and  $\langle (V-R) \rangle = 1.15$  mag. Using these values, we derive a visual absorption  $A_V = 0.35$  mag from LkCa-21's V-R excess compared to a M3.5 dwarf. This leads to a bolometric luminosity  $\log(L_{bol}/L_{\odot}) = -0.15$ , which locates the star on the  $0.35M_{\odot}$  Hayashi track in the H-R diagram. Hartmann et al. (1987) noted that LkCa-21 may be a spectroscopic binary

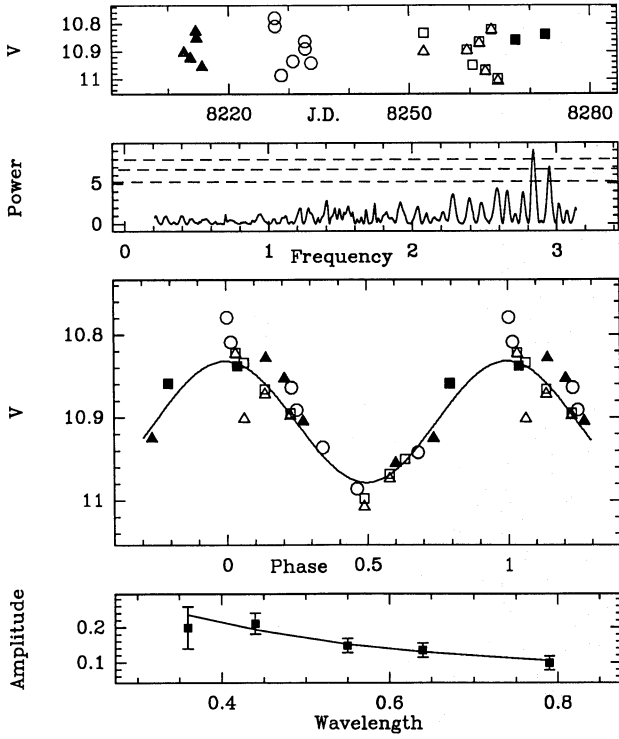


Fig. 20. LkCa-19. Panels are as in Fig. 4

on the basis of a discrepant radial velocity relative to the cloud's velocity.

LkCa-21's light curve in the V-band is shown in Fig. 21a while the corresponding periodogram is displayed in Fig. 21b. A strong peak appears at a period of 8.8d but only in the V and I periodograms, not in the R periodogram. The U- and B-band light curves were not included in the analysis because the star is too faint at these wavelengths. The string-length method also exhibits a 8.8d minimum in the V and I bands. The phased light curve in the V-band is shown in Fig. 21c and is well reproduced by a sinusoid. We did not attempt to apply the spot model on the light variations of LkCa-21 because we lack reliable U and B light curves. Moreover, we show in Sect. 3.1, that the assumption that the 8.8d period results from the modulation by spots conflicts with the large  $v \sin i$  measured for this star.

#### 2.4.6. TAP 9 (HBC 351)

The optical counterpart of TAP 9 (034903+2431) is a relatively rapidly rotating ( $v \sin i = 29 \text{ km s}^{-1}$ ) WTTS of spectral type K5 according to Walter et al. (1988). Leinert et al. (1992) report the existence of a companion at a distance of  $0.61''$  with a brightness ratio of 0.22 in the K-band.

The V-band light curve (Fig. 22a) reveals small amplitude ( $\Delta V = 0.1 \text{ mag}$ ) but rapid variations from one night to the other. If due to rotational modulation, this photometric behavior suggests a short rotational period. We therefore extended the interval of periods to be scanned down to 1.2 days. Four peaks reach the 90% confidence level in the V-band periodogram (Fig. 22b) and

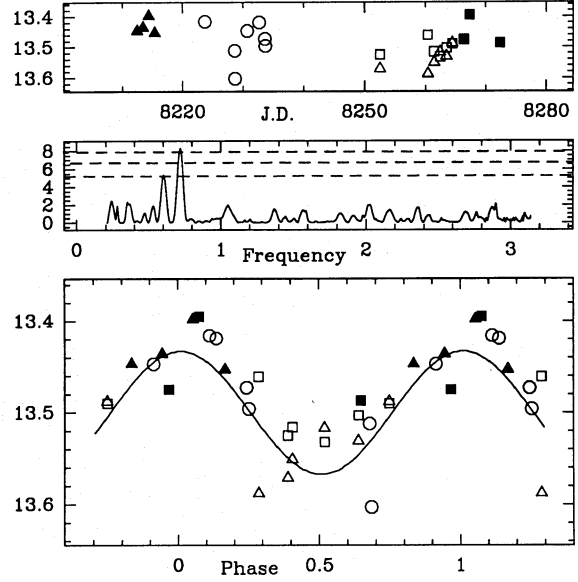


Fig. 21. LkCa-21. Panels are as in Fig. 1

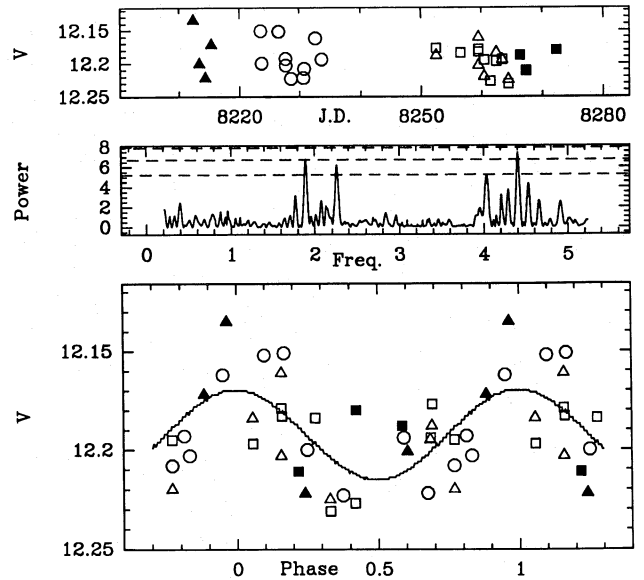


Fig. 22. TAP 9. Panels are as in Fig. 1

correspond to periods of 1.43, 1.56, 2.78, and 3.32 days, respectively. These four periods are very similar, though not strictly equal, to those found in SU Aur's light curve. We therefore conclude, as for SU Aur (see Sect. 2.3.13), that TAP 9's rotational period is very probably shorter than 3.5 days. For illustration purposes, a V-band light curve folded in phase with a period of 1.56d is shown in Fig. 22c. Owing to the large scatter of the phased light curves around the sine-curve fit added to the fact that we lack a reliable U-band light curve for this object, we did not attempt to apply the spot model.

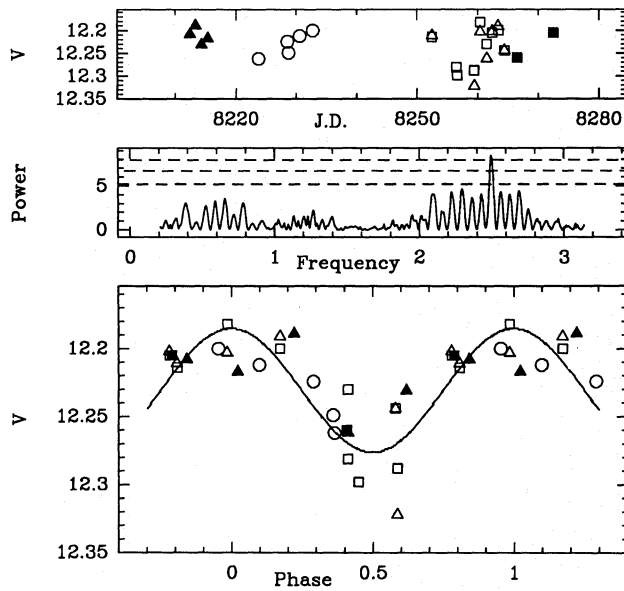


Fig. 23. TAP 26. Panels are as in Fig. 1

## 2.4.7. TAP 26 (HBC 376)

The optical counterpart of TAP 26 is a rapidly rotating ( $v \sin i = 68 \text{ km s}^{-1}$ ), WTTS of spectral type K7 (Walter et al. 1988). The V-band light curve (Fig. 23a) reveals photometric variations of small amplitude ( $\Delta V \simeq 0.1 \text{ mag}$  peak-to-peak) on a timescale of a few days. The BVR periodograms (Fig. 23b) exhibit a single peak above the 90% confidence level which corresponds to a period of 2.5 days. The phased light curve is shown in Fig. 23c. The low-level variability ( $\Delta m \leq 0.1 \text{ mag}$  in all bands) combined with the lack of a U-band light curve and the existence of a large scatter in the I-band prevented us to derive the amplitudes of the light variations over a wide enough wavelength range to warrant the application of the spot model. Moreover, we show below (Sect. 3.1) that the photometric period cannot be due to rotational modulation as it would imply a true equatorial velocity of  $28.5 \text{ km s}^{-1}$  while TAP 26's  $v \sin i$  amounts to  $68 \text{ km s}^{-1}$ .

## 2.4.8. TAP 40 (HBC 392)

The optical counterpart of this X-ray source first detected by Feigelson et al. (1987) is a K5 star with very weak  $H_\alpha$  emission ( $\text{EW}(H_\alpha) = 0.2 \text{ \AA}$ , Walter et al. 1988). The star maintained a roughly constant mean light level during the whole observing run (Fig. 24a) with photometric variations reaching an amplitude of  $0.1 \text{ mag}$  in the V-band. The BVRI periodograms (Fig. 24b) indicate a period of 3.35d with a confidence level larger than 99%, while the U-band light curve was not analyzed due to large measurement uncertainties ( $\langle U \rangle = 14.8$ ). The V-band light curve folded in phase with this period is displayed in Fig. 24c and is well fitted by a sinusoid. The BVRI amplitudes of the quasi-sinusoidal light variations are plotted in Fig. 24d and are well reproduced by a model indicating a spot temperature of  $3270 \text{ K}$  ( $T_{\text{eff}} = 4395 \text{ K}$ ) and a spot fractional area of 4%.

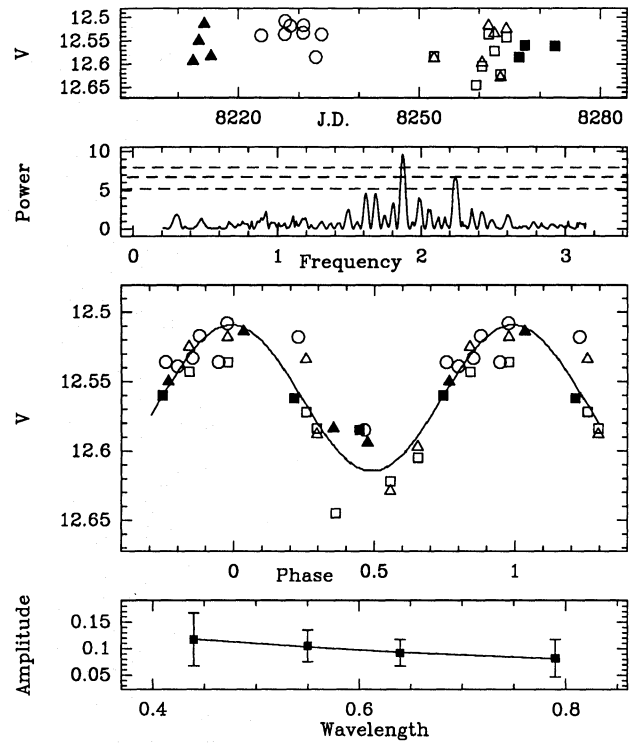


Fig. 24. TAP 40. Panels are as in Fig. 4

## 2.4.9. TAP 41 (HBC 397)

A low-luminosity K7 star, the optical counterpart of TAP 41 (042916+1751) is a very weak line TTS with moderate rotation ( $v \sin i = 27 \text{ km s}^{-1}$ , Walter et al. 1988). The amplitude of photometric variability did not exceed  $0.1 \text{ mag}$  in the V-band during our observations (Fig. 25a). No significant peak is found simultaneously in at least 2 colors in the periodogram when exploring a range of possible periods between 2 to 30 days (the strong, low-frequency peak seen at  $P = 8.7 \text{ d}$  in the V-band periodogram shown in Fig. 25b does not appear at other wavelengths). By extending this range down to 1.1 days, we find only one peak at a period of 1.21d that reaches close to or above the 90% confidence level at 3 wavelengths (BVR, Fig. 25b). Yet, the string-length method does not reveal any significant period in this range. The V-band light curve folded in phase with a period of 1.21d is shown in Fig. 25c and exhibits a large scatter around the sine curve fit. Although the B and R light curves display more sinusoidal variations than the V light curve, the tentative 1.21d period needs to be confirmed by further observations. Because of all these uncertainties added to the lack of a U-band light curve, no model fitting was attempted.

## 2.4.10. TAP 57NW (HBC 427)

A visual binary lies at the position of the X-ray source TAP 57 (Feigelson et al. 1987). The north-west component has been identified as a weak-line TTS which is itself a single-lined spectroscopic binary (Mathieu et al. 1989). TAP 57NW's light curve in the V-band is shown in Fig. 26a. The periodogram analysis



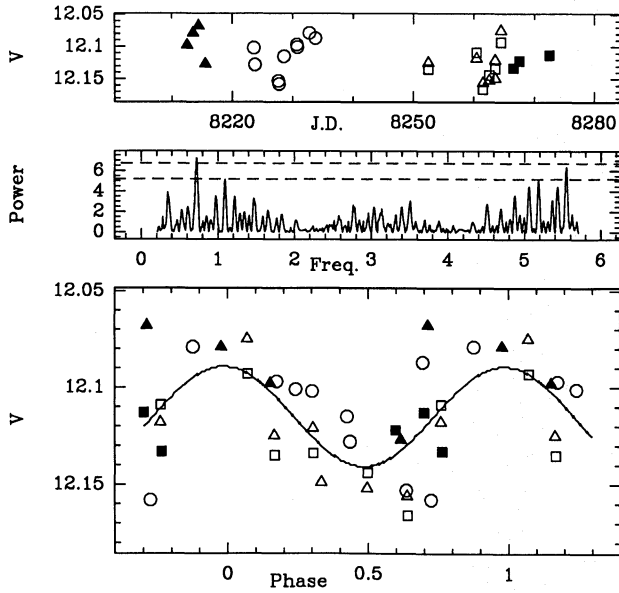


Fig. 25. TAP 41. Panels are as in Fig. 1

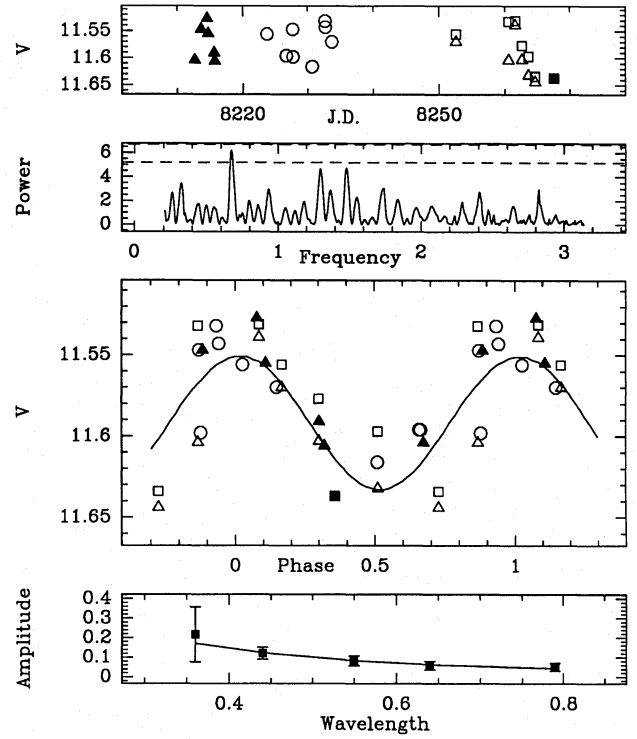


Fig. 26. TAP 57NW. Panels are as in Fig. 4

reveals only one peak reaching above the 90% confidence level in 2 colors (U and B) for a period of 4.22d, which appears below the 90% confidence level in the V-band periodogram shown in Fig. 26b, while the string-length method indicates a deep minimum at a period of 4.7d in the U, B, and V bands. The minimum is still seen in the R and I bands although not as deep as in the other colors. A V-band light curve folded in phase with  $P=4.7$ d is shown in Fig. 26c.

Assuming that the observed variability is due to the modulation of the stellar flux by surface spots, we applied the spot model to the amplitudes of the light variations from U to I (Fig. 26d). We find that the amplitudes are best reproduced by spots hotter than the photosphere ( $T_{spot}=4650$ K,  $T_{eff}=4000$ K) that cover only 2% of the stellar surface. The presence of hot spots on such a weakly active TTS is an unexpected result. Since TAP 57NW is a spectroscopic binary, the model solution may be affected by the presence of the companion if it significantly contributes to the total luminosity of the system at optical wavelengths. Lacking any constraint on the luminosity ratio between the star and its companion, we cannot assess the significance of this result.

### 3. Discussion

In this section, we first discuss the origin of the photometric periods detected in the light curve of our TTS sample by comparing the stellar projected velocity,  $v \sin i$ , with the true equatorial velocity deduced from the photometric period. We briefly discuss the general properties of the spots located at the surface of TTS and then focus on the rotational properties of these stars.

#### 3.1. The origin of the photometric periods

In order to check whether the photometric periods derived above result from the rotational modulation of the stellar flux by surface spots and thus reflect the rotational period of the star, we computed the corresponding equatorial velocity ( $V_{eq}=2\pi R_*/P$ ) using the values of stellar radius listed in Table 1. The projected velocity,  $v \sin i$ , is plotted against the equatorial velocity in Fig. 27. For most stars in our sample, the stellar radius was deduced from the stellar bolometric luminosity and the stellar effective temperature as listed by Strom et al. (1989a). The stellar bolometric luminosity was derived by these authors after having corrected the observed spectral energy distribution for non-stellar flux excesses. Plotting  $v \sin i$  against  $V_{eq}$  is in fact equivalent to plotting  $R_* \sin i$  versus  $R_*$ , so that Fig. 27 also provides a check to the validity of the stellar radii derived in this way.  $V_{eq}$  and  $v \sin i$  are listed in Table 1 for our stellar sample. BD +24°676 does not appear in Fig. 27 as its  $v \sin i$  is unknown. We argued above (Sect. 2.3.1) that the light variations of this star are induced by orbital rather than rotational motion.

It is seen from Fig. 27 that the majority of the stars have  $v \sin i$  less than  $V_{eq}$  as expected. However, 5 stars (DG Tau, RY Tau, GM Aur, LkCa-21, TAP 26) have a larger  $v \sin i$  than  $V_{eq}$ , while 2 other stars (SU Aur, TAP 9) only have an upper limit set on their rotational period so that the  $V_{eq}$  plotted in Fig. 27 is a lower limit. These 7 stars are discussed below.

Lower limits on the equatorial velocities of SU Aur and TAP 9 in Fig. 27 were computed assuming an upper limit of 3.5d on their rotational period. We actually found 4 possible

**Table 1.** Photometric period, stellar radius, true and projected equatorial velocities of stars of the COYOTES sample

Star	Period (d)	$R_*$ ( $R_\odot$ )	$R_*$ ref.	$V_{eq}$ ( $\text{km s}^{-1}$ )	$v \sin i$ ( $\text{km s}^{-1}$ )	$v \sin i$ ref.
Classical TTS						
DE Tau	7.6	2.6	st	17.2	10.0	hs
DF Tau	8.5	3.0	st	17.9	$16.1 \pm 5.3$	hs
DG Tau	6.3	2.1	bb	16.5	$21.7 \pm 6.3$	hs
DI Tau	7.5	2.3	st	15.3	10.5	hs
DK Tau	8.4	2.6	st	15.9	11.4	hs
DR Tau	2.8, 7.3	1.6	bb	29, 11	$\leq 10$	hs
GG Tau	10.3	2.6	st	12.9	10.2	hs
GK Tau	4.65	2.2	st	23.8	$18.7 \pm 3.5$	hs
IP Tau	3.25	1.5	st	23.4	$\leq 11.0$	hss
RY Tau	24.0 <sup>†</sup>	1.8	st	3.8	$52.2 \pm 1.8$	hs
GM Aur	12.0	1.9	st	8.0	$12.4 \pm 1.8$	hs
SU Aur	$\leq 3.5$	3.1	st	$\geq 45.3$	$65.0 \pm 3.5$	hs
LkCa-15	5.85	1.6	hvr	13.9	$12.5 \pm 1.3$	hss
Weak-line TTS						
IW Tau	5.6	2.4	st	22.0	$\leq 9.0$	b
LkCa-4	3.37	2.2	st	32.9	$26.1 \pm 2.4$	hss
LkCa-7	5.64	2.0	st	18.0	$13.0 \pm 3.0$	b
LkCa-19	2.24	1.5	wa, st	33.6	$18.6 \pm 1.9$	hss
LkCa-21	8.8 <sup>†</sup>	2.6	tw	15.0	$60 \pm 11$	hss
TAP 9	$\leq 3.5$	1.2	st	$\geq 17.4$	29	wa
TAP 26	2.51 <sup>†</sup>	1.4	st	28.5	68	wa
TAP 40	3.38	1.1	st	16.3	17	wa
TAP 41	1.21	1.7	st	70.2	27	wa
TAP 57 NW	4.70	2.2	st	23.4	10	b

<sup>†</sup> Not the rotational period (see text)

References to Table 1: bb: Basri & Bertout (1989), b: Bouvier (unpublished), hs: Hartmann & Stauffer (1989), hss: Hartmann et al. (1987), hvr: Herbig, Vrba, Rydgren (1986), st: Strom et al. (1989a), tw: this work, wa: Walter et al. (1988).

rotational periods for these two stars: 1.45, 1.57, 2.78, and 3.35 days. Comparison between  $v \sin i$  and the equatorial velocities derived from these periods indicates that all but the longest period (3.35d) lead to an equatorial velocity consistent with the measured  $v \sin i$  allowing for a 20% error on the stellar radius determination. In turn, these rotational periods would imply a true equatorial velocity of  $56 \text{ km s}^{-1}$  or more for SU Aur, which is not unreasonable for a  $2M_\odot$  star, and of  $22 \text{ km s}^{-1}$  or more for TAP 9.

Two other stars (DG Tau and GM Aur) have an equatorial velocity which is marginally consistent with the measured  $v \sin i$ . DG Tau's  $V_{eq}$  of  $16.5 \text{ km s}^{-1}$  actually agrees with a  $v \sin i$  of  $21.7 \pm 6.3 \text{ km s}^{-1}$  (Hartmann & Stauffer 1989) within the error bars. The lower limit on  $v \sin i$  ( $15.4 \text{ km s}^{-1}$ ) implies an axial inclination of  $70^\circ$  or larger. For GM Aur, we deduce an equatorial velocity of  $8.0 \text{ km s}^{-1}$  from the 12.0d photometric period, while  $v \sin i = 12.4 \pm 1.8 \text{ km s}^{-1}$  (Hartmann & Stauffer 1989). The difference between  $V_{eq}$  and the lower limit of  $v \sin i$  is only 2.6

$\text{km s}^{-1}$ , and could easily arise from a 20% error on the estimate of the stellar radius. In any case, comparison between  $V_{eq}$  and  $v \sin i$  indicates that the inclination angle of GM Aur's rotational axis is close to  $90^\circ$ , a result which strengthens Kardoplov's (1989) claim that GM Aur is an eclipsing binary system.

The equatorial velocity of the three remaining stars (RY Tau, LkCa-21, TAP 26) cannot be reconciled with the measured  $v \sin i$ , even accounting for errors on  $v \sin i$  and stellar radius determinations. TAP 26's large  $v \sin i$  ( $68 \text{ km s}^{-1}$ , Walter et al. 1988) implies a rotational period of the order of 1.0 days, which would be undetectable from the night-to-night sampling of the COYOTES light curve. The 2.5d photometric period detected for that star may correspond to the orbital motion of a binary system. The same explanation might hold for RY Tau and LkCa-21 as the former was once reported to be a radial velocity variable (Herbig 1977) while the radial velocity of the latter is significantly different from the velocity of the associated molecular cloud (Hartmann et al. 1987). In any case, it is clear that the

**Table 2.** Rotational periods and spots properties

Star	Period (d)	$T_{eff}$ (°K)	$T_{spot}^{\dagger}$ (°K)	Area <sup>†</sup> (%)
Classical TTS				
DE Tau	7.6	3680	4770	1.3
DF Tau	8.5	3800	5140	3
DG Tau	6.3	3920	3430 <sup>1</sup>	15
			4850 <sup>2</sup>	15
DK Tau	8.4	4000	2410	25
GG Tau	10.3	4000	3030	7
GK Tau	4.65	4000	4810	30
IP Tau	3.25	3920	4930	3
GM Aur	12.0	4000	5810	0.7
SU Aur	≤3.5	5770	5670	21
LkCa-15	5.85	4395	3010	22
Weak-line TTS				
IW Tau	5.6	4000	3295	7
LkCa-4	3.37	4000	3035	8
LkCa-7	5.64	4000	2490	11
LkCa-19	2.24	5240	4770	13
TAP 40	3.38	4395	3270	4
TAP 57 NW	4.70	4000	4650	2

<sup>†</sup> The properties of spots hotter than the photosphere are listed in italics for clarity  
<sup>1</sup> No veiling.  
<sup>2</sup> With veiling (see text).

photometric periods measured for these three stars do not correspond to the stellar rotational period.

We conclude that the photometric periods derived for TTS in the present study are compatible with rotational periods for all but three stars (RY Tau, LkCa-21, TAP 26). The mean  $\sin i$  is 0.62 for WTTS and 0.79 for CTTS, the latter value being close to the expected value of 0.785 for randomly oriented rotational axes, while the former is smaller. According to a two-sided Kolmogorov-Smirnov test, there is a 77% probability that the distribution of rotational axis of CTTS in our sample is random, while the probability is only 5% for WTTS. These results, however, must be viewed with caution, owing to the small sample size. Weaver (1987) investigated in a similar way the distribution of axial inclination in a sample of 20 TTS and found a 0.02% chance that the inclinations are distributed at random. The discrepancy between Weaver's and our results (see also Bouvier 1991) most likely comes from a systematic overestimation of the luminosity of the sample stars in the former study, which leads to an underestimated axial inclination as discussed by Weaver (1987).

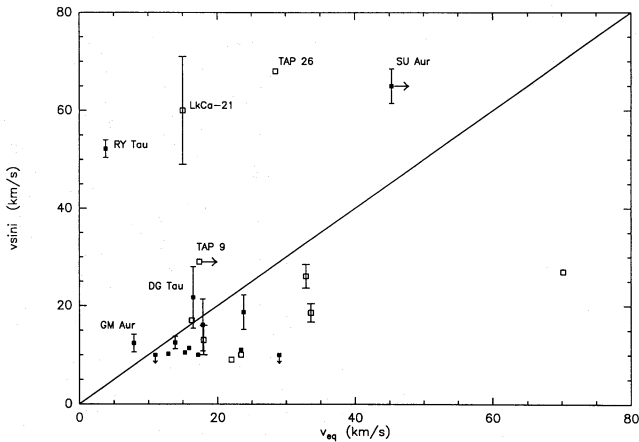


**Fig. 27.** The projected equatorial velocity is plotted versus the true equatorial velocity deduced from the rotational period for WTTS (empty squares) and CTTS (filled squares). Vertical bars indicate the uncertainty on  $v \sin i$  when available. Horizontal arrows for SU Aur and TAP 9 represent lower limits on the equatorial velocity. Two points with vertical arrows indicating a  $10 \text{ km s}^{-1}$  upper limit on  $v \sin i$  are plotted for DR Tau, which correspond to the two photometric periods detected for this star (see text). Stars are expected to lie below the  $v \sin i = v_{eq}$  line (solid line) if their photometric period is due to rotational modulation. Stars lying above this line are identified by their names (see text)

### 3.2. Spots properties

The spots properties derived for the stars whose light variations could be modeled are listed in Table 2. In spite of the uncertainties on the spot modeling (see Sect. 2.2), a few general trends seem to emerge for the average properties of CTTS and WTTS spots. As a basis for the discussion, Fig. 28 displays the temperature difference between the photosphere and the spots as a function of the stellar effective temperature. Three groups can be identified in this Fig.: i) stars with spots hotter than the photosphere by approximately 1000K (Group I); ii) stars with spots cooler than the photosphere by approximately 1000K (Group II); and two stars of earlier spectral types (LkCa 19 and SU Aur) in which the temperature difference between the spots and the photosphere is significantly lower than in TTS of later spectral types. These two stars exhibit small amplitudes of variability and, since they have a similar spot coverage as the other stars of the sample (see Table 2), this seems to result from a lower contrast between the spots and the photosphere.

Of the 7 stars in Group I, 6 are classical TTS and 1 a WTTS. The WTTS, TAP 57NW, is known to be a binary system (Mathieu et al. 1989), so that the derived spots properties may be affected by the presence of the companion. Unambiguous evidence for hot spots has been found in only 3 CTTS so far: DF Tau (Bouvier & Bertout 1989 and Sect. 2.3.3. above), DN Tau (Vrba et al. 1986), and BP Tau (Vrba et al. 1986; Simon et al. 1990). Within the uncertainties of the present spot model, the results are consistent with the hypothesis that hot spots are found exclusively in CTTS, not in WTTS. This strengthens the interpretation put forward by Bertout et al. (1988) that hot spots are



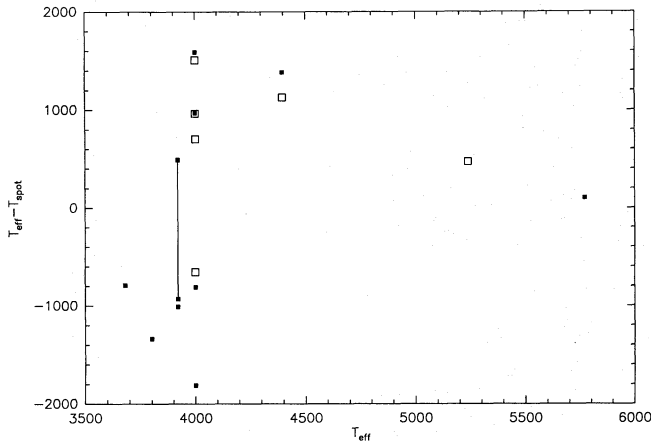


**Fig. 28.** The temperature difference between the photosphere and the spots is plotted against the stellar effective temperature for WTTS (empty squares) and CTTS (filled squares). The two points connected by a solid line correspond to the spot solutions found for DG Tau with and without veiling included in the spot model, respectively

shock-excited regions near the stellar surface that result from the accretion of circumstellar material channeled along the stellar magnetic field lines. On average, hot spots are found to be less extended than cool ones, with a fractional coverage of typically a few percent of the stellar surface (see Table 2), though the largest one is found to occupy 30% of GK Tau's surface.

Stars of Group II include as many WTTS as CTTS. Within our restricted sample, the properties of cool spots in CTTS and WTTS are undistinguishable. The spots have a temperature approximately 1000K lower than that of the photosphere and cover from 4% to typically 25% of the stellar surface. These figures are similar to those derived previously by Bouvier & Bertout (1989) which led them to suggest that TTS cool spots are the stellar analogues of sunspots, albeit on a much larger scale. There is, however, a striking difference between WTTS's and CTTS's light curves. When folded in phase, the former exhibit much less scatter around a sine-curve fit than the latter (see Figs. 2c to 26c). In fact, the observed scatter in the folded light curves of WTTS is most often comparable to the scatter expected from measurement errors alone. Hence, the photometric behavior of WTTS on a timescale of a few weeks can usually be understood as a pure modulation of the stellar flux by surface spots. In contrast, CTTS light curves include two components: a light modulation by surface spots as in WTTS and a presumably irregular variability of lower amplitude.

At any rate, the fact that we detected rotational modulation in the light curves of 20 TTS among the 23 we monitored indicates that spots are indeed the primary cause of the photometric variations of both WTTS and CTTS on a timescale of a few weeks. Moreover, that WTTS light curves exhibit a small scatter around a sine-curve fit indicates that the lifetime of cool spots is larger than the observing period of about 2 months. Both the spots' position at the stellar surface and the spots' properties remained constant during the whole observing period as indicated

by the lack of a phase shift as well as by the constant amplitudes of photometric variations. The lifetime of cool spots might in fact be much longer than 2 months as Vrba et al. (1988) found that spots persisted for several years at the surface of the WTTS V410 Tau with only a slight change in position. Similarly, since we were able to detect the rotational modulation induced by hot spots over our observing period, some hot spots must have a lifetime of the order of a few weeks at least. However, the larger scatter exhibited by CTTS light curves may indicate that hot spots' properties and/or their position at the stellar surface change on a shorter timescale. This must be the case for DF Tau in our sample since the previously reported 8.5d period is found only in segments of its light curve, and not in the overall light curve. Another striking case reported by Simon et al. (1990) is BP Tau which exhibited a 7.6d period during 3 weeks, then went through a quiescent state for 2 weeks, and eventually resumed its periodic photometric behavior but with a period of 6.1 days. It thus appears that hot spots may not be as stable as cool spots at the surface of TTS, a result which is consistent with the hypothesis that cool and hot spots have different origins, namely stellar magnetism for the former, magnetically-channeled accretion of circumstellar material for the latter.

### 3.3. Rotational periods

#### 3.3.1. Overall distribution

The rotational periods detected during the COYOTES campaign range from 1.2 to 12.0 days. The lower limit of 1.2 days is probably a selection effect since shorter periods would be very difficult to detect from light curves sampled on a night-to-night basis. On the contrary, the upper limit of 12.0 days is certainly real and not merely an observational bias since we are able to detect periods up to at least 30 days. Moreover, one of the goals of the COYOTES campaign was to derive the rotational periods of stars with low  $v \sin i$  in order to check whether these stars really are very slow rotators or merely moderate rotators seen at low axial inclination. Therefore, our sample is not biased toward fast rotators but contains 10 stars with a  $v \sin i$  of the order of  $10 \text{ km s}^{-1}$  or less. These are: DE Tau, DI Tau, DK Tau, DR Tau, GG Tau, IP Tau, LkCa-15, IW Tau, LkCa-7, TAP 57NW. The equatorial velocity of these stars derived from their rotational period ranges from  $12.9$  to  $23.7 \text{ km s}^{-1}$  (see Table 1), quite typical of the average rotational velocity of low-mass TTS (see Bouvier 1991). This result confirms Bouvier et al.'s (1986b) claim that intrinsically slow rotators, with an equatorial velocity much less than  $10 \text{ km s}^{-1}$ , are nonexistent or very rare among T Tauri stars with an age less than  $5 \times 10^6 \text{ yr}$ . Since our stellar sample is biased toward relatively luminous TTS (see below), it might be that very slow rotators have to be searched for among older, less luminous T Tauri stars which have not been included in photometric monitoring programs so far because of their faintness.

In the following sections, we discuss the relationships between rotational period and various stellar properties. The stellar properties of TTS from the COYOTES sample are listed in

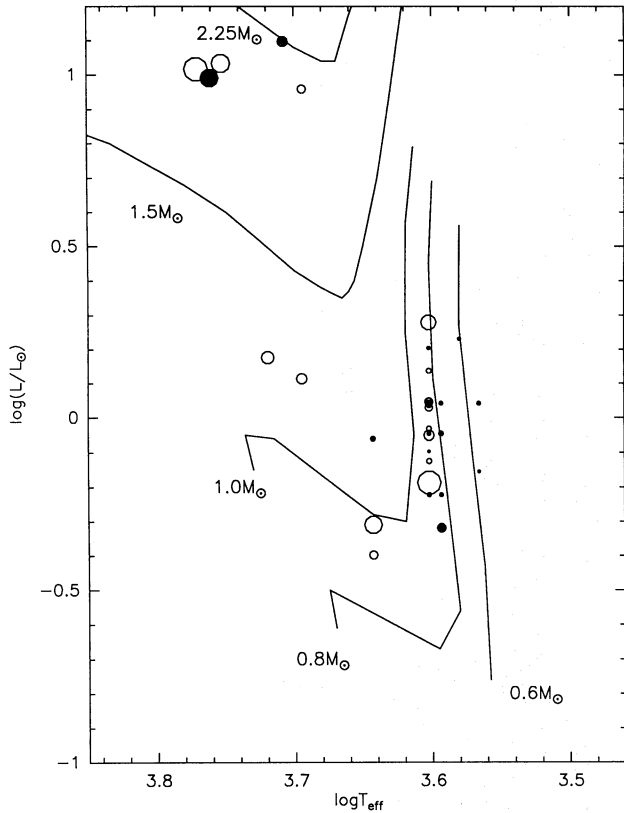


**Fig. 29.** WTTS (empty circles) and CTTS (filled circles) of the Taurus-Auriga cloud with known rotational periods are plotted in the H-R diagram. The size of the circles is proportional to the stellar angular velocity. Solid lines show evolutionary tracks for 0.6, 0.8, 1.0, 1.5, and  $2.25M_{\odot}$  stars, respectively

Table 3. In order to increase the statistical significance of the discussion, we add to the periods derived above for 19 stars of the COYOTES sample (DR Tau is excluded since it exhibits two possible rotational periods) those published for 17 other TTS belonging to the Taurus-Auriga association. This secondary sample includes 10 WTTS and 7 CTTS, whose rotational periods and stellar properties are listed in Table 4.

### 3.3.2. Rotational period and stellar mass: WTTS vs CTTS

The extended sample (Tables 3 and 4) includes 36 stars, 18 CTTS and 18 WTTS, whose location in the H-R diagram is shown in Fig. 29. Stars are represented in this figure by symbols whose size is proportional to the stellar angular velocity ( $\Omega = 2\pi/P$ ). It is apparent from this diagram that, on the average, less massive TTS tend to be slower rotators than more massive ones. That the rotation rate of TTS statistically increases with stellar mass was first demonstrated by Vogel & Kuhl (1981) based on  $v \sin i$  measurements. Rotational period measurements now provide an opportunity to study this correlation more accurately since, unlike  $v \sin i$ , rotational periods are not affected by projection effects. In Fig. 30, the rotational period is plotted as a function of the stellar effective temperature. The maximum rota-

tional period smoothly increases from about 2 days for G2 stars ( $M \approx 2M_{\odot}$ ) to more than 10 days for K7-M0 stars ( $M \approx 0.9M_{\odot}$ ). For an average stellar radius of 2 solar radii, this corresponds to an increase of the minimum equatorial velocity from 10 km s<sup>-1</sup> for  $0.9M_{\odot}$  stars to 51 km s<sup>-1</sup> for  $2M_{\odot}$  ones.

The insufficient number of stars with a spectral type earlier than K0 in our sample does not allow us to derive the scatter in rotational period among intermediate-mass stars. This is not the case for low-mass TTS, however, and a striking feature of Fig. 30 is the large scatter in rotational period at a given mass among these stars. In particular, the 26 K7-M1 stars with a mass between 0.6 and  $0.9M_{\odot}$  ( $\log T_{eff} = 3.566$  to 3.602) have rotational periods spanning the whole observed range from 1.2 to 12 days. Moreover, it is seen from Fig. 30 that the scatter is clearly non-random in the sense that classical TTS tend to have longer periods than weak-line TTS. Histograms of the rotational periods of WTTS and CTTS in this mass range are compared in Fig. 31. The mean rotational period of the 15 CTTS is 7.6 days with a  $1\sigma$  deviation of 2.1 days, while it is  $4.1 \pm 1.7$  days for the 11 WTTS. A two-sided Kolmogorov-Smirnov test confirms that the two distributions are different at the 99.9% probability level.

A few stars in these histograms have an ambiguous status. This is the case of V410 Tau whose spectral type is K7 in the red spectral range (Cohen & Kuhl 1979), but K3-K4 in the blue one (Bouvier et al. 1986b; Basri et al. 1991). If a K7 star, its mass is  $0.9M_{\odot}$ . However, if a K4 star, it has a mass of  $1.1M_{\odot}$ , and is then expected to rotate faster than the other, lower-mass stars in the histogram. Another case is DI Tau which we classified as a CTTS while its present-day spectral properties would suggest a WTTS (see Sect. 2.3.5.). Finally, DF Tau, DL Tau, and DE Tau have a spectral type M0.5, M1, and M1, respectively, while all the other stars in the histograms have a K7 or M0 spectral type. In order to check whether these 5 stars could introduce a significant bias in the histograms we repeated the Kolmogorov-Smirnov test after having removed V410 Tau, DF Tau, DL Tau and DE Tau from the distributions, i.e., considering only stars with a well-defined spectral type of K7 or M0, and after having moved DI Tau from the CTTS to the WTTS distribution. The test still indicates that the two distributions are different at the 97.7% confidence level. Therefore, the difference of rotational period between WTTS and CTTS in our sample is a robust result.

It is interesting to note that V836 Tau, a WTTS, has a rotational period ( $P=7.0$  days) more typical of a CTTS. Conversely, IP Tau was classified as a CTTS but its rotational period ( $P=3.2$  days) is more typical of that of a WTTS. It turns out that these two objects have spectral characteristics which place them at the (arbitrary) border between WTTS and CTTS. Both have a moderate  $H_{\alpha}$  equivalent width (9 and 10 Å, respectively) but exhibit a significant near-IR excess (Strom et al. 1989a). Therefore, their classification as WTTS or CTTS is uncertain. We note that removing these stars from the histograms, or switching them from one distribution to the other, would result in an even larger difference between the 2 distributions.

The difference between the mean rotational period of WTTS and CTTS amounts to less than a factor of two. This might ex-

**Table 3.** Rotational periods and stellar properties for the COYOTES sample

Star	Period (d)	$L_*$ ( $L_\odot$ )	Sp.T.	$T_{eff}$ °K	EW(Li) Å	EW(H $\alpha$ ) Å	$\Delta K$ dex
CTTS							
DE Tau	7.6	1.1	M1	3680.	.99	54	.22
DF Tau	8.5	1.7	M0.5	3800.	.79	54	.41
DG Tau	6.3	0.9 <sup>1</sup>	M0 <sup>1</sup>	3920.	.51	113	—
DI Tau	7.5	1.1	M0	3920.	—	2	.01
DK Tau	8.4	1.6	K7	4000.	.65	19	.43
GG Tau	10.3	1.6	K7	4000.	.72	55	.36
GK Tau	4.65	1.1	K7	4000.	—	16	.49
IP Tau	3.25	0.5	M0	3920.	—	10	.31
GM Aur	12.0	0.8	K7	4000.	.50	97	.09
SU Aur	1.6	9.8	G2	5770.	.24	4	.41
LkCa 15	5.85	0.9 <sup>2</sup>	K5	4395.	—	13	—
WTTS							
IW Tau	5.6	1.4	K7	4000.	—	4	-.03
LkCa 4	3.37	1.1	K7	4000.	.51	5	.07
LkCa 7	5.64	0.9	K7	4000.	.60	4	.14
LkCa 19	2.24	1.5 <sup>3</sup>	K0	5240.	.44	0.5	—
TAP 9	1.6	0.5	K5	4395.	.37	1.6	.14
TAP 40	3.38	0.4	K5	4395.	.15	0.2	.05
TAP 41	1.21	0.65	K7	4000.	—	0.5	.09
TAP 57NW	4.7	1.1	K7	4000.	.58	0.7	.06

Except where noted, the source for  $L_*$ , Sp.T., EW(H $\alpha$ ) and  $\Delta K$  is Strom et al. (1989a) and references therein. The source for EW(Li) is Basri et al. (1991)

<sup>1</sup> Basri & Bertout (1989)

<sup>2</sup> Herbig et al. (1986)

<sup>3</sup> Walter et al. (1988)

plain why previous studies failed to detect any significant difference between CTTS's and WTTS's  $v \sin i$  distributions (Hartmann et al. 1987; Hartmann & Stauffer 1989; Bouvier 1990a). Such a small difference could conceivably be masked by the uncertainties on  $v \sin i$  which arise both from the unknown  $\sin i$  and from the fact that, for low-mass TTS,  $v \sin i$  is often close to or even lower than the detection limit of  $10 \text{ km s}^{-1}$ . In order to test whether such an explanation holds for our sample, we applied a two-sided Kolmogorov-Smirnov test to the  $v \sin i$  distributions of the CTTS and WTTS subsamples. The test indicates a probability of 63% that the two distributions are different, a rather inconclusive result.

In any case, direct rotational period measurements leave no doubt as to the existence of a different rotational regime for WTTS and CTTS in our sample. In the next 3 sections, we discuss possible origins for this difference.

### 3.3.3. Selection effects

We discuss in this section the possibility that the WTTS and CTTS subsamples used here are affected by selection effects in

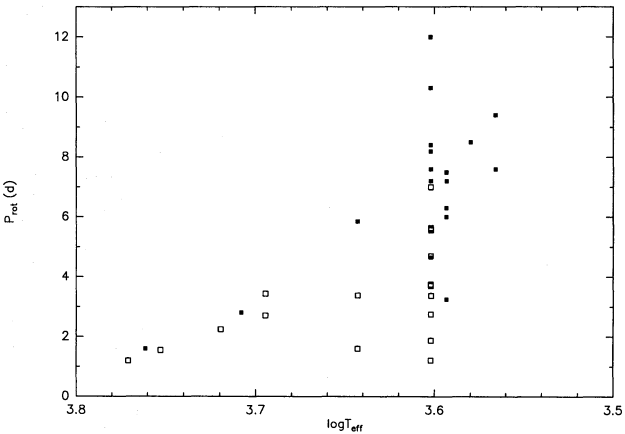


**Fig. 30.** The rotational period is plotted versus the stellar effective temperature for WTTS (empty squares) and CTTS (filled squares). Note the apparent increase of the maximum rotational period towards lower effective temperatures as well as the large scatter of rotational period among K7 stars ( $\log T_{eff}=3.602$ )

**Table 4.** Rotational periods and stellar properties for the additional sample

Star	Period (d)	Source	$L_{\star}$ ( $L_{\odot}$ )	Sp.T.	$T_{eff}$ °K	EW(Li) Å	EW(H $\alpha$ ) Å	$\Delta K$ dex
CTTS								
DN Tau	6.0	b86	.9	M0	3920.	.65	12	.21
BP Tau	7.6	vr86	.9	K7	4000.	.69	40	.26
DH Tau	7.2	vr89	.6	M0	3920.	—	53	.29
GI Tau	7.2	vr86	.9	K7	4000.	—	19	.49
AA Tau	8.2	vr89	.6	K7	4000.	.64	37	.33
DL Tau	9.4	sh91	.7	M1	3680.	.80	105	—
T Tau	2.8	he86	12.5	K1	5105.	.34	38	.42
WTTS								
V410 Tau	1.87	vr88	1.9	K7	4000.	.42	2.1	.13
UX Tau A	2.7	bo86	1.3	K2	4950.	.42	3.9	.44
HP Tau/G2	1.2	vr89	10.4	G0	5900.	—	4.5	.01
V773 Tau	3.43	rv83	9.1	K2	4950.	.47	1.5	.10
V819 Tau	5.6	bo86, ry84	.75	K7	4000.	—	1.7	.19
V826 Tau	3.7	bo86	1.07	K7	4000.	—	1.6	.06
V827 Tau	3.75	bo86	1.11	K7	4000.	.57	1.8	.14
V830 Tau	2.75	bo86	.89	K7	4000.	—	3.0	.07
V836 Tau	7.0	ry84	.60	K7	4000.	.57	9.0	.16
HDE 283572	1.55	wa87	10.81	G5	5660.	—	abs.	-.05

The source for  $L_{\star}$ , Sp.T., EW(H $\alpha$ ) and  $\Delta K$  is Strom et al. (1989a) and references therein, except for DL Tau whose luminosity and spectral type are from Basri & Bertout (1989). The source for EW(Li) is Basri et al. (1991)  
References to Table 4: b86: Bouvier et al. (1986a), bo86: Bouvier et al. (1986b), he86: Herbst et al. (1986), rv83: Rydgren & Vrba (1983), ry84: Rydgren et al. (1984), sh91: Shevchenko et al. (1991), vr86: Vrba et al. (1986), vr88: Vrba et al. (1988), vr89: Vrba et al. (1989), wa87: Walter et al. (1987).

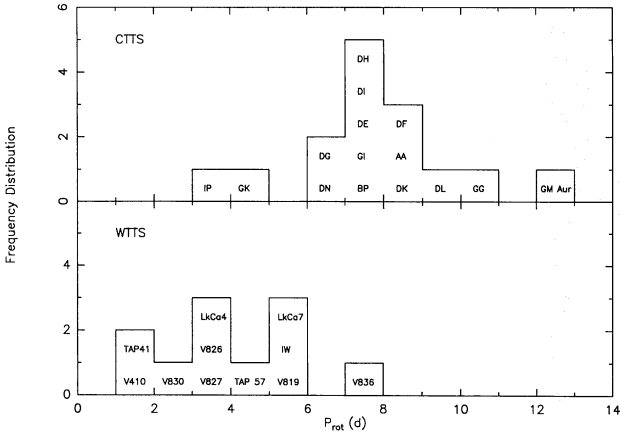


**Fig. 31.** Frequency distributions of the rotational periods of CTTS (top) and WTTS (bottom). Only stars with a spectral type from K7 to M1 are represented and identified by their names. The two distributions are different at the 99.9% confidence level, indicating that WTTS are faster rotators than CTTS

such a way that the former is biased toward fast rotators and the latter towards slow rotators. Because long-term photometric monitoring campaigns are usually performed with relatively small telescopes, the primary selection criterion is the star's brightness. For the COYOTES campaign, only stars with a V-magnitude of 13.5 or lower were retained and the location of the stars of the additional sample in the H-R diagram (Fig. 29) shows that the same criterion applied for their selection. Hence, the whole sample is biased toward relatively luminous TTS. However, it is seen from Fig. 29 that WTTS and CTTS have similar luminosities, so that the bias does not affect the comparison between the two subsamples.

Another bias may arise from the very method used to identify CTTS and WTTS. CTTS included in the present sample were first detected during H $\alpha$  surveys of the Taurus-Auriga cloud. In contrast, the large majority of the presently known WTTS have been detected during X-ray surveys of the cloud (Feigelson et al. 1987; Walter et al. 1988) and some others during Herbig's et al. (1986) Ca II H and K survey of the same cloud. The existence of a correlation between X-ray flux and rotation in TTS (Bouvier 1990b) then raises the concern that X-ray surveys are biased toward the detection of fast rotators, and would be un-



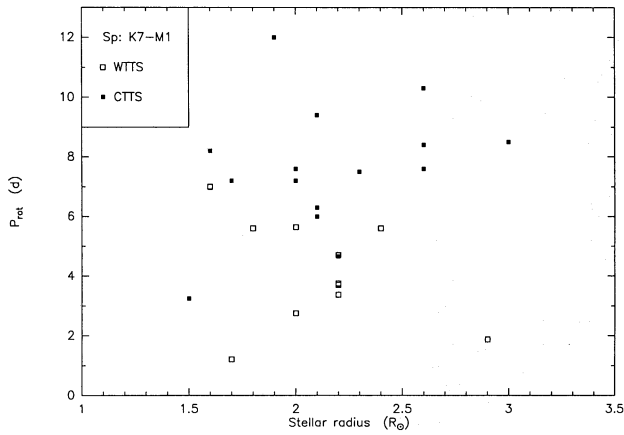


**Fig. 32.** The rotational period of K7-M1 WTTS (empty squares) and CTTS (filled squares) is plotted as a function of the stellar radius. No correlation appears between the two quantities

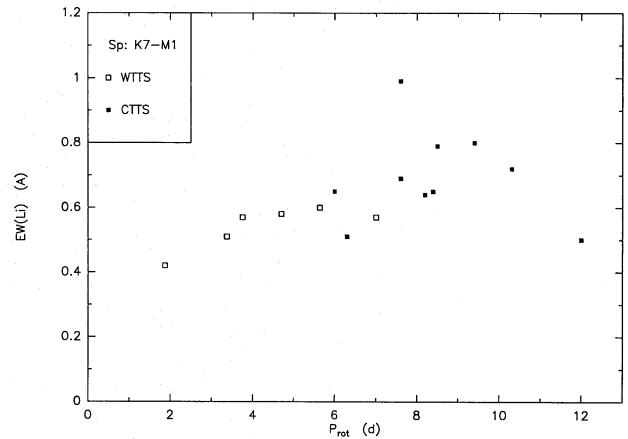


**Fig. 33.** The LiI  $\lambda 6707$  equivalent width is plotted against the rotational period for K7-M1 WTTS (empty squares) and CTTS (filled squares)

able to reveal PMS stars characterized by slow rotation and low  $H_{\alpha}$  emission. The existence of such a population of PMS stars seems, however, excluded by recent proper motion surveys of the Taurus-Auriga cloud (Hartmann et al. 1991; Gomez et al. 1992) which discovered only 9 new PMS stars down to a magnitude limit of 15.5. It therefore appears that the presently known  $H_{\alpha}$  selected CTTS and X-ray or otherwise selected WTTS are representative of the whole PMS population of the cloud.

We therefore conclude that the only bias that affects our sample results from the selection of relatively bright TTS, but this does not affect the comparison between the rotational period distributions of WTTS and CTTS.

### 3.3.4. Rotational period and age

Could the difference in rotation rate between WTTS and CTTS result from a difference in age? If convective stars on their Hayashi tracks evolve without angular momentum loss, homologous contraction leads to a change of the rotational period inversely proportional to the square of the stellar radius. If attributed to an evolutionary effect, and assuming a mean age of  $2.10^6$  yr for CTTS, the difference in rotational period would imply an age of  $6.10^6$  yr for WTTS. However, it is readily seen from Fig. 29 that WTTS and CTTS along the  $0.9M_{\odot}$  Hayashi track do not show any evidence for rotational evolution. A plot of the rotational period as a function of stellar radius for TTS with a spectral type between K7 and M1 (Fig. 32) confirms the lack of a correlation between these two quantities.

More generally, WTTS are known to share the same region of the H-R diagram as CTTS, a result which is often called upon to argue for their similar age. Yet, several complications arise when trying to determine the ages, even relative, of WTTS and CTTS. First, the location of classical T Tauri stars in the H-R diagram is uncertain due to the continuum excesses of non-stellar origin that contribute to the total luminosity of the object from UV to IR wavelengths. Various attempts have been made to remove this extra-stellar contribution in order to derive

the true stellar luminosity (e.g. Strom et al. 1989a) but they rely on assumptions that are questionable at least for the most active CTTS (e.g., that there is no significant continuum excess at optical wavelengths). Second, as pointed out by Hartmann & Kenyon (1990), accretion of circumstellar material at the stellar surface may result in an evolutionary path in the H-R diagram that significantly departs from standard Hayashi tracks. As a consequence, the identical location of WTTS and CTTS in the H-R diagram would not necessarily point to a similar evolutionary status.

Another argument sometimes used to support the coevality of WTTS and CTTS is that the two subclasses exhibit roughly the same range of lithium abundances (e.g. Basri et al. 1991). However, the processes responsible for lithium depletion during PMS evolution are still poorly understood. In fact, the lithium abundances measured for TTS do not comply with theoretical expectations from standard models (Basri et al. 1991; Strom et al. 1989b; Magazzù et al. 1992), a result which suggests that parameters other than age, e.g. rotation and/or mass-accretion, play a role in the lithium depletion rate.

In order to investigate the possible effect of rotation upon lithium depletion, we plotted in Fig. 33 the LiI  $\lambda 6707$  equivalent width versus the rotational period for stars of our sample. Only stars with a spectral type between K7 and M1 have been considered. There is a hint of a correlation ( $r=0.46$ ) between  $EW(Li)$  and  $P_{rot}$  in the sense that, on average, CTTS have both longer periods and a larger lithium equivalent width than WTTS. Such a correlation may indicate that rapid rotation leads to a faster lithium depletion rate as it induces more mixing in the stellar interior. In that case, the overall  $EW(Li)$ - $P_{rot}$  correlation would be consistent with WTTS and CTTS having the same age but different lithium abundances because the lithium depletion rate primarily depends upon rotation. We note, however, the absence of a correlation between these two quantities *within* each subclass. Therefore, the overall correlation may as well be interpreted as indicating that CTTS are systematically younger than WTTS and therefore have had less time to deplete

lithium, regardless of their rotation rate. Still another possibility is that accretion of lithium-rich circumstellar material from the disk leads to a replenishment of fresh lithium at the surface of CTTS. In other words, we are not able to disentangle in such a correlation the effects that age, disk accretion, and/or rotation may have onto the lithium depletion rate in young stars.

Clearly, the issue of the relative ages of CTTS and WTTS is not settled yet, so that the possibility that the different rotation rate between CTTS and WTTS is due to an age effect, the latter being slightly older than the former, cannot be totally dismissed at this point. However, we show below (see Sect. 3.4.) that it is difficult to understand the rotational evolution of young stars up to the ZAMS in the framework of this hypothesis.

### 3.3.5. Rotation, accretion, and mass-loss

Alternatively, the origin of the lower rotation rates of CTTS compared to WTTS may be searched for in the fact that, unlike WTTS, CTTS possess energetic winds and accretion disks. The weak  $H_\alpha$  emission of WTTS as well as the absence of detectable forbidden-line emission in their spectra suggests a mass-loss rate of less than  $10^{-9} M_\odot \text{yr}^{-1}$  in these stars (Edwards et al. 1992). Assuming  $\dot{M} \simeq 10^{-10} M_\odot \text{yr}^{-1}$ , the braking timescale of WTTS estimated from conventional models may thus be as long as a few  $10^8$  years (Bouvier 1991), i.e., much larger than their contraction timescale. Therefore, WTTS are expected to spin up as they contract on their Hayashi track as indicated by theoretical models of the evolution of stellar angular momentum in solar-type stars (e.g. Pinsonneault et al. 1990). The rotational evolution of CTTS is much more complex owing to the possible influence of mass-accretion and strong mass-loss. Hartmann & Stauffer (1989) showed that, in the absence of angular momentum loss, accretion of circumstellar material on the stellar surface at a rate of  $10^{-7} M_\odot \text{yr}^{-1}$  would spin up the central star to half the break-up velocity in a few  $10^6$  yrs. Since CTTS rotate at typically 1/10 of the break-up velocity, they proposed that the strong wind carries away the angular momentum excess in these stars. In support of this hypothesis, Cabrit et al. (1990) reported the existence of a tight correlation between mass-accretion and mass-loss diagnostics in CTTS, which suggests that the gravitational energy released during the accretion process is the ultimate energy source for driving the energetic winds. Typical accretion rates derived for CTTS range from a few  $10^{-9}$  to a few  $10^{-7} M_\odot \text{yr}^{-1}$  (Bertout et al. 1988; Basri & Bertout 1989) while mass-loss rates range from  $10^{-9}$  to  $10^{-7} M_\odot \text{yr}^{-1}$  (Edwards et al. 1987). The existence of a proportionality between mass-accretion and mass-loss, as suggested by Cabrit et al.'s (1990) correlation, may at least qualitatively account for the restricted range of rotational periods observed in CTTS and for the fact that CTTS are prevented from spinning up while accreting from their disk on the Hayashi tracks. The detailed mechanism by which the winds are powered is, however, unknown. Recent models suggest that a magnetic coupling between the central star and the inner disk regions may be the origin of the wind (Camenzind 1990; Königl 1991). These models further indicate that if the star's magnetosphere disrupts the disk beyond

the corotation radius, the star may actually be braked rather than spun up by the accretion process.

Cameron & Campbell (1992) performed numerical simulations along these lines and concluded that for values thought to be typical of the surface magnetic field and accretion rates in CTTS ( $B_o = 500\text{G}$  to  $1\text{kG}$ , and  $\dot{M} = 3 \cdot 10^{-8} M_\odot \text{yr}^{-1}$ , respectively), the magnetic coupling between the star and the disk leads to a quasi-static equilibrium where the star evolves at almost constant angular velocity. According to their simulations, the equilibrium period is reached in less than  $3 \cdot 10^6$  yrs and ranges from 2.5 to 13.0 days, in good agreement with the periods observed for our sample stars. Most likely, current models of rotational braking by the disk are oversimplified. For instance, the central assumption that the strong stellar magnetic field that threads the inner disk regions has a dipolar structure is probably unrealistic. It remains to be seen whether this mechanism can work with the more chaotic field structure at the stellar surface that seems warranted by various diagnostics such as, e.g., strong X-ray flares indicating the existence of large magnetic loops extending several stellar radii away from the stellar surface (Montmerle et al. 1983), the lack of a detection from polarization measurements of an organized magnetic field stronger than a few hundred gauss (Babcock 1958; Brown & Landstreet 1981), and the very existence of cool, non-polar magnetic spots at the stellar surface (Bouvier & Bertout 1989). Besides, the fate of the circumstellar material at the disk disruption radius is not addressed in Cameron & Campbell's model. Instead, the model assumes that when the disk is disrupted beyond the corotation radius the angular momentum of the circumstellar material does not reach the stellar surface. The validity of such an assumption has yet to be proven by fully consistent MHD models.

Clues to the impact of disk accretion and mass-loss on the rotational evolution of CTTS may be searched for by investigating correlations between rotational period and accretion or mass-loss diagnostics. The most direct diagnostic of mass-loss in CTTS is forbidden line emission, such as [OI], [SII], and [NII] (Edwards et al. 1987, 1991). Cabrit et al. (1990) showed that forbidden line emission is tightly correlated with  $H_\alpha$  line emission. Therefore, the latter can empirically be used as a surrogate for the former even though Calvet & Hartmann (1992) recently suggested that part of the  $H_\alpha$  line emission may occur in the infalling rather than outflowing material near the star. Because  $H_\alpha$  emission has been measured for all the stars of our sample while forbidden line emission has not, we use here the  $H_\alpha$  line equivalent width as a measure of the mass-loss rate. Various diagnostics have been proposed to quantify the mass-accretion rate and most are related to the magnitude of the IR excess exhibited by TTS (see Edwards et al. 1991). Only part of the observed IR excess, however, derives from the dissipation of gravitational energy during the accretion process. Another contribution comes from the reprocessing of stellar photons in the optically thick disk regions, so that even passive disks, in which no accretion takes place, lead to some IR excess (Kenyon & Hartmann 1987). Other diagnostics such as optical veiling or UV excess are more directly linked to the accretion process but have been measured for fewer stars than the IR diagnostics and

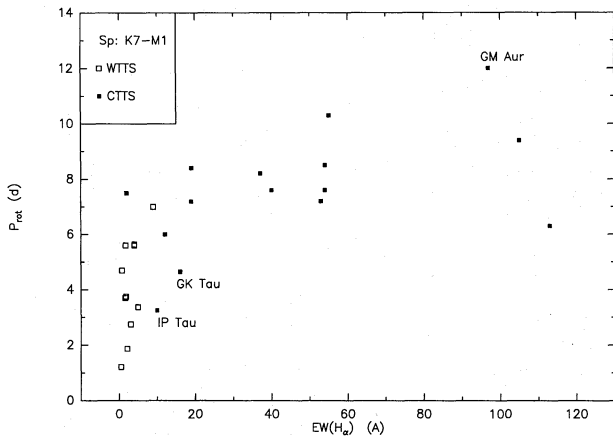


**Fig. 34.** The rotational period of K7-M1 WTTs (empty squares) and CTTS (filled squares) is plotted against the  $H_\alpha$  line equivalent width

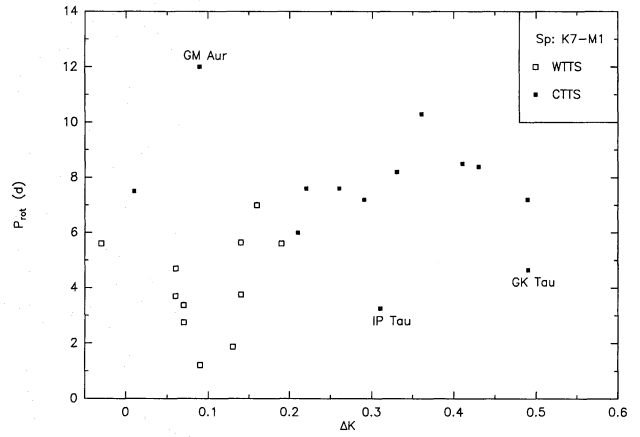


**Fig. 35.** The rotational period of K7-M1 WTTs (empty squares) and CTTS (filled squares) is plotted against  $\Delta K$ , the IR excess at  $2.2\mu\text{m}$

are known to be extremely variable on short timescales (e.g. Basri & Batalha 1991). Therefore, we adopt here  $\Delta K$ , the IR excess at  $2.2\mu\text{m}$ , as measured by Strom et al. (1989) for many TTS, to quantify the mass-accretion rate.

The rotational period is plotted versus the  $H_\alpha$  equivalent width for the K7-M1 TTS sample in Fig. 34. As expected from the distribution of their rotational periods, CTTS and WTTs cluster into two well-separated regions of the diagram: 12 out of 13 stars with  $\text{EW}(H_\alpha) > 10\text{\AA}$  have  $P_{\text{rot}} \geq 6$  days while among the 13 stars with  $\text{EW}(H_\alpha) \leq 10\text{\AA}$ , 11 have a rotational period shorter than 6 days. Yet, when considering WTTs and CTTS separately, no correlation is found between  $\text{EW}(H_\alpha)$  and  $P_{\text{rot}}$  within either of the two subclasses. On the contrary, the rotational period appears fairly constant and independent of  $H_\alpha$  emission for stars with  $\text{EW}(H_\alpha)$  from  $20\text{\AA}$  to  $120\text{\AA}$ .

In Fig. 35, the rotational period is plotted against the IR excess at K. The results are similar to those obtained when comparing the rotational period to the  $H_\alpha$  equivalent width, namely: most stars with a K-excess larger than 0.2 mag have a rotational period longer than 6 days, while most of those with a K-excess less than 0.2 mag have rotational periods shorter than 6 days. Again, there is no significant correlation between the two quantities when considering the WTTs and the CTTS subsamples separately. The scatter is somewhat larger in this figure than in the previous one, especially among WTTs, and most probably results from larger measurement uncertainties for the K-excess, especially for K-excess values less than 0.2, than for  $\text{EW}(H_\alpha)$ .

Figures 34 and 35 thus suggest that the rotational period of most CTTS is roughly constant and independent of either  $\text{EW}(H_\alpha)$  or  $\Delta K$ . This is consistent with the hypothesis that mass-loss rate scales with mass-accretion rate in CTTS as suggested by Cabrit et al. (1990), so that the wind carries away the angular momentum excess of the disk material accreted onto the star. Nevertheless, 3 stars (GM Aur, GK Tau, and IP Tau) seem to significantly depart from the rest of the CTTS sample in the  $P_{\text{rot}}-\Delta K$  diagram and, to a lesser extent, also in the  $P_{\text{rot}}-H_\alpha$

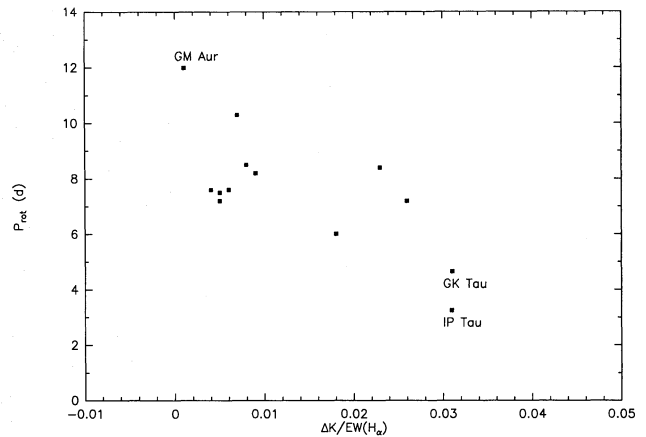


**Fig. 36.** The rotational period of K7-M1 CTTS is plotted against the parameter  $\Delta K/\text{EW}(H_\alpha)$ , which is a measure of the relative importance of accretion compared to mass-loss in CTTS (see text)

diagram. More precisely, GM Aur lies above the other CTTS in the two diagrams, while the reverse is true for IP Tau and GK Tau. It turns out that these 3 stars lie in the tails of the rotational period distribution of CTTS, GM Aur being the slowest rotator of our CTTS sample, while IP Tau and GK Tau are the fastest ones (see Fig. 31).

Although Cabrit et al. (1990) demonstrated the existence of a general correlation between IR excess and  $H_\alpha$  emission in TTS, Strom et al. (1989) pointed out that a few stars significantly depart from that correlation. This is the case for GM Aur which exhibits strong  $H_\alpha$  emission but a weak continuum excess at  $2.2\mu\text{m}$ . GM Aur's spectral energy distribution is peculiar in the sense that it exhibits a small excess at 2.2 microns but has a strong excess at wavelengths larger than 10 microns. Strom et al. (1989) speculated that such a peculiar IR energy distribution pertains to objects that are near the end of their accretion phase and started to clear the inner part of their circumstellar disks. If correct, that GM Aur is the slowest rotator of our sample would suggest that the star was spun down while accreting



from its circumstellar disk. Alternatively, Cabrit et al. (1990) interpreted the near-IR excess deficiency of GM Aur as indicating that the star is seen almost edge-on, so that the inner parts of its accretion disk, where the near-IR excess arises, are hidden from the observer. This interpretation is supported by the high value we found above for GM Aur's inclination angle as well as by Kardoplov's (1989) claim that GM Aur may be an eclipsing binary. Hence, GM Aur's intrinsic near-IR excess may be much larger than what is actually observed.

Conversely, the fastest two rotators, GK Tau and IP Tau, have a large near-IR excess but exhibit small  $H_\alpha$  emission. In fact, these two stars have the largest  $\Delta(K)/EW(H_\alpha)$  ratio of the whole sample while the slowest rotator, GM Aur, has the smallest one. If  $\Delta(K)$  correctly parametrizes the mass-accretion rate while  $EW(H_\alpha)$  is a wind diagnostic, the  $\Delta(K)/EW(H_\alpha)$  ratio is a measure of the relative importance of accretion to mass-loss processes in CTTS. The large  $\Delta(K)/EW(H_\alpha)$  ratio of GK Tau and IP Tau would thus suggest that accretion dominates over mass-loss in these two stars as compared to other TTS of the sample, and this may account for their shorter than average rotational period. Conversely, the small  $\Delta(K)/EW(H_\alpha)$  ratio in GM Aur suggests that the braking torque from the wind is more important relative to the accretion torque in this star than in the other CTTS in our sample, which may explain why GM Aur is the slowest rotator of the sample. In order to further test this hypothesis, we plotted the rotational period versus the  $\Delta(K)/EW(H_\alpha)$  ratio in Fig. 36. Although a suggestive trend, consistent with the above interpretation, does appear ( $r=0.73$ ), it is clear that there is no one-to-one correspondence between the value of the rotational period and the  $\Delta(K)/EW(H_\alpha)$  ratio within this limited sample.

The results above are consistent with the hypothesis that most CTTS have reached a state of quasi-static equilibrium where the braking torque due to the wind balances the accelerating torque due to disk accretion, so that the star evolves at nearly constant angular velocity on its Hayashi track. This equilibrium may also result from the magnetic coupling between the star and the disk as suggested by recent models (e.g. Cameron & Campbell 1992). The existence of such an equilibrium would account for the observed Gaussian-shaped distribution of rotational periods of CTTS, which exhibits a fairly small scatter around the mean value ( $\sigma/P=0.26$ ). In comparison, the rotational period distribution of WTTS is relatively flat within statistical uncertainties and exhibits a larger scatter ( $\sigma/P=0.41$ ). It would also explain why CTTS rotate more slowly than WTTS as the latter spin up during their contraction on their Hayashi track while the former are prevented to do so. We speculate that the few stars that form the low- and high-velocity tails of the rotational period distribution of CTTS may correspond to objects where accretion dominates over mass-loss for rapid rotators, or the opposite for slow rotators. The origin of such an imbalance between mass-accretion and mass-loss has yet to be identified.

### 3.4. Implications for the rotational evolution to the main sequence

The results obtained above shed new light onto the angular momentum evolution of young stars up to the ZAMS. It has been known since the mid-80's that, while  $1M_\odot$  TTS have rotational velocities in the range from less than  $10\text{km s}^{-1}$  up to about  $30\text{km s}^{-1}$ , solar-mass ZAMS stars in young stellar clusters exhibit a much larger range of  $v\sin i$ , from less than  $10\text{km s}^{-1}$  up to  $150\text{km s}^{-1}$  (Stauffer et al. 1987; Stauffer et al. 1989a; Stauffer et al. 1989b). More precisely, in a young cluster such as  $\alpha$  Persei (age:  $5 \cdot 10^7$  yr), approximately half of the  $1M_\odot$  ZAMS dwarfs are slow rotators with  $v\sin i$  less than  $10\text{km s}^{-1}$ , while the other half are "fast" rotators with a  $v\sin i$  larger than  $20\text{km s}^{-1}$  and up to  $150\text{km s}^{-1}$  (Prosser 1991). The question then arises: assuming that TTS are the progenitors of ZAMS stars in young clusters, how to account for the peculiar rotational distribution of ZAMS stars starting from that of TTS?

Theoretical models describing the evolution of stellar angular momentum prior to the main sequence have been developed to address this issue (Pinsonneault et al. 1989, 1990; MacGregor 1991). The models indicate that PMS stars spin up on radiative tracks as their moment of inertia decreases and thus may arrive onto the ZAMS with a rotation rate similar to that observed for the fastest ZAMS rotators if only a small amount of angular momentum is lost during this phase. In this case, however, the extremely small  $v\sin i$  of the other half of ZAMS stars cannot be accounted for. Conversely, assuming a significant amount of angular momentum loss during the PMS contraction phase, one may account for the slow ZAMS rotators but not for the fastest ones. In other words, the difficulty is more to explain the *whole range* of  $v\sin i$  observed among ZAMS stars than to account for the *mean* velocity of these stars (see Bouvier 1991); and because theoretical models had only limited success in this respect so far, this problem triggered a number of speculations as to which physical mechanisms could account for the evolution of the rotational spectrum of TTS stars into that observed for ZAMS stars (Stauffer & Hartmann 1987; Hartmann & Stauffer 1989; Bouvier 1990a; Bouvier 1991).

The results obtained in the present study suggest that WTTS and CTTS may have quite a different rotational evolution on their Hayashi tracks. It is therefore tempting to identify the two populations of rotators among ZAMS stars with the two TTS subclasses. More precisely, we argue in the following that WTTS are the progenitors of the ZAMS fast rotators, while the CTTS are the progenitors of the slow rotators.

First, conventional models of magnetic braking suggest that the braking timescale of WTTS may be as long as  $1.5 \cdot 10^8$  years, i.e., much larger than the contraction timescale to the ZAMS, if their mass-loss rate is as low as  $10^{-10} M_\odot \text{yr}^{-1}$  (Bouvier 1991). This is consistent with the results of theoretical models (Pinsonneault et al. 1989, 1990; MacGregor 1991) that indicate that *diskless* PMS stars will spin up while contracting onto their Hayashi and radiative tracks. The reduction of the moment of inertia of a  $1M_\odot$  star between an age of  $3 \cdot 10^6$  years and the ZAMS is a factor of 6.3 according to Pinsonneault et al.'s (1990) evolution-



ary models. Therefore, starting with a mean rotational period of 4.0 days in the T Tauri phase, a WTTS would reach the ZAMS with a rotational period of 0.6 days, which corresponds to an equatorial velocity of  $80 \text{ km s}^{-1}$ . Such short rotational periods have indeed been measured for the rapid rotators of the Pleiades cluster (Van Leeuwen & Alphenaar 1982). Hence, considering the whole range of rotational periods observed for WTTS, it is possible to reproduce the range of rotational velocities observed for fast rotators in young clusters.

Second, we argued above that CTTS are prevented from spinning up on their convective tracks up to the point where their circumstellar disk dissipates. According to Strom et al. (1989a) and Skrutskie et al. (1990), the disk survival time does not exceed  $10^7$  years. For a  $1M_{\odot}$  star, this age corresponds to the point where the star reaches the radiative part of its evolutionary track. From thereon, its rotational evolution will be the same as the one of a WTTS, i.e., it will spin up as its moment of inertia decreases. According to Pinsonneault et al.'s (1990) models, the stellar moment of inertia of a  $1M_{\odot}$  star decreases by a factor of 3 between  $10^7$  years and  $3 \cdot 10^7$  years. Then, assuming a mean rotational period of 8.0 days at the end of the Hayashi evolution, the star will reach the ZAMS with a rotational period of about 2.5 days, which corresponds to a rotational velocity of  $20 \text{ km s}^{-1}$ . This is much larger than the upper limit of  $10 \text{ km s}^{-1}$  observed for a large fraction of stars in young clusters. Therefore, if CTTS really are the progenitors of the slowly rotating ZAMS stars, they must not only be prevented from spinning up on their Hayashi track but indeed be braked and reach the end of the Hayashi track with a rotational period of 15 days or longer. An obvious test of this scenario will be to measure the rotational periods of CTTS near the end of their Hayashi evolution.

We thus propose that WTTS are continuously accelerated as they contract towards the main sequence, while CTTS are first braked on their convective track, then spun up on their radiative track. A consequence of this hypothesis is that the majority of the slow rotators observed in young clusters such as  $\alpha$  Persei *never were* rapid rotators. This is at odds with current models describing the rotational history of the Sun (Pinsonneault et al. 1990) which assume that the Sun once was a rapidly rotating ZAMS star, suddenly braked once on the main sequence. A major problem encountered by these models is that they predict the existence a large radial velocity gradient in the present-day Sun, while observations indicate an almost constant angular velocity in the solar interior down to  $0.2R_{\odot}$  (Libbrecht 1989). We note that this problem is readily solved if the Sun never was a rapidly rotating star.

Clues to the rotational evolution of young stars may also be gained from the analysis of the abundances of light elements at their surface. Balachandran et al. (1988) found a “correlation” between lithium abundance and rotation in ZAMS stars of the  $\alpha$  Persei cluster, in the sense that slow rotators display a very wide range of Li abundances, from cosmic to strongly depleted, while rapid rotators only exhibit cosmic Li abundances. We believe that this “correlation” can be understood, albeit very qualitatively at this point, in the framework of our hypothesis as we now show.

The lithium depletion rate depends upon the amount of mixing in the stellar interior, which, in turn, is believed to scale with the amount of internal differential rotation. According to our scenario, WTTS and CTTS both spin-up on radiative tracks leading to fast and slow rotators on the ZAMS, respectively. There is no uncoupling between the inner radiative core and the outer convective envelope during this phase of evolution, so that the amount of internal differential rotation, as well as the lithium depletion rate, is minimized. Therefore, both fast and slow rotators are expected to exhibit close to cosmic lithium abundances as they arrive onto the ZAMS. This would account for the nearly cosmic abundances observed for all the fast rotators and for a fraction of the slow rotators in the  $\alpha$  Persei cluster. Once on the ZAMS, fast rotators are rapidly spun-down to velocities similar to those of slow rotators (Stauffer & Soderblom 1991). The usual interpretation for such a sudden deceleration is that only the outer convective envelope is braked while the inner radiative core remains in rapid rotation. Since the braking affects only the outer convective envelope, it induces extra-mixing at the core-envelope boundary and leads to a rapid Li depletion. We thus suggest that the fraction of  $\alpha$  Persei slow rotators which exhibit low lithium abundances initially were rapid rotators quickly spun-down on the ZAMS. Balachandran et al. (1988) similarly speculated that the correlation between lithium abundance and rotation could result from a combination of an age spread among the cluster stars and a large dispersion in their initial angular momentum distribution though they could not trace the origin of this dispersion.

Finally, we note that the comparison between the rotational distributions of TTS and ZAMS stars casts strong doubt onto the possibility that the lower rotation rates of CTTS compared to those of WTTS is an age effect as discussed in Sect. 3.3.4. above. Assuming that WTTS rotate faster than CTTS because the former are slightly more evolved than the latter would lead to the conclusion that the rotation rate of PMS stars monotonously increases from the TTS phase up to the ZAMS, which is difficult to reconcile with the existence of slowly rotating stars in young open clusters.

#### 4. Summary and conclusion

The main results of the present study are as follow:

- 1) Rotational modulation of the stellar luminosity by surface spots is detected in 20 out of 24 stars monitored over a time interval of 2 months. This high detection rate indicate that spots are the primary cause of the photometric variability of TTS, WTTS and CTTS alike, on a timescale of days to weeks.

- 2) Within the uncertainties of our spot model, the rotational modulation seems to exclusively result from the presence of spots cooler than the photosphere in WTTS while both cool and hot spots appear to exist at the surface of CTTS.

- 3) The photometric behavior of WTTS on a timescale of weeks is consistent with pure rotational modulation by spots. Although this is also the dominant source of variability for CTTS, an additional, low-level and presumably irregular source of light variations is present in these stars.

4) The rotational periods of our sample stars range from 1.2 to 12.0 days. The longest rotational period corresponds to an equatorial velocity of  $8\text{ km s}^{-1}$ , which confirms the paucity of extremely slow rotators, with  $v\sin i < 10\text{ km s}^{-1}$ , among TTS with an age less than  $5 \times 10^6$  yrs.

5) The *maximum* rotational period increases towards lower mass stars, from about 2.0d at  $M=2M_{\odot}$  to 12.0d at  $M=0.9M_{\odot}$ . This is consistent with the results of extensive  $v\sin i$  studies that show that the average rotational velocity of TTS increases with stellar mass.

6) There is a seemingly large scatter in rotational periods for stars in the mass range from 0.7 to  $0.9M_{\odot}$ . However, much of the scatter results from the systematically lower rotation rates of CTTS compared to WTTS. The mean rotational period of 11 K7-M1 WTTS is  $4.1 \pm 1.7$  d while it is  $7.6 \pm 2.1$  d for 15 CTTS in the same mass range. The distribution of rotational periods for WTTS and CTTS in this mass range are different at the 99.9% confidence level. We interpret this difference as indicating that WTTS spin up as they contract on their Hayashi tracks while CTTS are prevented to do so.

7) When considered separately, K7-M1 WTTS and CTTS exhibit a relatively small scatter around the subclasses' mean rotational period, which indicates a dispersion of less than a factor of 3 in angular momentum in each subclass.

8) According to our interpretation, the difference of rotational rate between WTTS and CTTS will increase with time as stars contract along their Hayashi track until CTTS disperse their disk. We suggest that the resulting angular momentum difference between WTTS and CTTS at the bottom of the Hayashi tracks is the origin of the wide range of rotational velocities observed for ZAMS solar-mass stars in young clusters. More specifically, we propose that WTTS are the progenitors of rapidly rotating young dwarfs and CTTS the progenitors of slowly rotating ones. A consequence of this hypothesis is that a large fraction of the slow rotators in a young cluster such as  $\alpha$  Persei never were rapid rotators.

Many central issues related to the rotational evolution of solar-mass PMS stars still have to be addressed. For instance, while the results of the present study suggest that accreting stars are prevented to spin up on their convective tracks, the detailed mechanism by which the star disposes of its angular momentum has yet to be identified. Forthcoming COYOTES campaigns, together with more direct determinations of mass-accretion and mass-loss rates in CTTS will help to constrain the models that describe the exchange of angular momentum between the star and its circumstellar environment. Another major issue is the relationship between CTTS and WTTS. While it appears that CTTS evolve into WTTS in a time less than  $10^7$  yrs, it is still unclear whether *all* WTTS are the offsprings of CTTS or whether some are stars that form without a circumstellar disk. Finally, we argued that the differing rotational evolution of WTTS and CTTS on their Hayashi tracks may ultimately lead to the wide range of rotational velocities observed for low-mass stars in young clusters. Yet, it remains to be seen how WTTS manage to spin up on their radiative tracks to reach a velocity of  $150\text{ km s}^{-1}$  on a timescale of  $3 \times 10^7$  yrs while, once on the ZAMS, they

are braked on a similar timescale down to velocities of less than  $10\text{ km s}^{-1}$ .

The present study was limited to stars belonging to the Taurus-Auriga stellar formation region. Attridge & Herbst (1992) conducted a similar photometric monitoring study of PMS stars in the Orion nebula cluster. They detect photometric periods in 35 stars and find the period distribution to be bimodal with a "fast" rotator group with a mean period of  $2.2 \pm 1.0$  d, and a "slow" rotator group with a mean rotational period of  $8.5 \pm 2.5$  d. Lacking spectroscopic observations of these stars, they are unable to identify the origin of this bimodality. We note that both the mean rotational period and the dispersion around the mean they derive for their slow and fast rotator groups are similar to the numbers we obtained above for WTTS and CTTS of the Taurus-Auriga cloud, respectively. We therefore suspect that the bimodal period distribution observed for stars of the Orion cluster at least partly results from the inclusion of both rapidly rotating WTTS and slowly rotating CTTS in Attridge and Herbst's stellar sample. Spectroscopic determination of the stellar properties of the Orion nebula cluster stars should soon provide a test of this hypothesis.

Several observational tests of our interpretation of the distribution of rotational periods among WTTS and CTTS are readily obtainable. For instance, photometric monitoring of TTS near the end of their Hayashi tracks should reveal CTTS rotating more slowly than those included in the present sample since we expect the distribution of CTTS rotational periods to shift towards longer periods as they contract on their Hayashi track. On the opposite, WTTS at the end of their Hayashi evolution should include even faster rotators than those detected in our sample. Another test will be provided by the photometric monitoring of PMS solar-mass stars on their radiative tracks which should reveal a wide range of rotational periods since we expect a fraction of these stars to be the offsprings of rapidly rotating WTTS while another fraction would correspond to slowly rotating CTTS that recently dispersed their disk. Finally, future COYOTES campaigns aimed at deriving the rotational periods of stars belonging to young clusters of slightly different ages will yield an observational mapping of the evolution of the angular momentum of low-mass stars near the main sequence. By providing strong constraints on theoretical models, such studies will help identifying the physical mechanisms that play a major role in the evolution of the stellar angular momentum prior to and on the main sequence.

**Acknowledgements.** We gratefully acknowledge fruitful discussions with S. Edwards on the rotational evolution of young stars. This work was partially supported by the Spanish Ministerio de Educación y Ciencia, Grant numbers PB 87/0387, PB 90/0167, and PB 91/0007. M.F. acknowledges her predoctoral fellowship of the Comunidad Autónoma de Madrid. J.M.M. is grateful for financial support from NSERC grants to A.F.J. Moffat and G.A.H. Walker.

## References

- Al-Naimy 1978, Ap. Sp. Sci. 53, 181
- Attridge J.M., Herbst W. 1992, ApJ Letters, in press

- Babcock H.W. 1958, ApJS 3, 141
- Balachandran S., Lambert D.L., Stauffer J.R. 1988, ApJ 333, 267
- Basri G., Batalha C. 1990, ApJ 363, 654
- Basri G., Bertout C. 1989, ApJ 341, 340
- Basri G., Martín E.L., Bertout C. 1991, A&A 252, 625
- Bertout C., Basri G., Bouvier J. 1988, ApJ 330, 350
- Bouvier J. 1990a, in: Rotation and Mixing in Stellar Interiors, eds. M.-J. Goupil & Zahn J.-P., p.47
- Bouvier J. 1990b, AJ 99, 946
- Bouvier J. 1991, in: Angular Momentum Evolution of Young Stars, eds. S. Catalano & J.R. Stauffer, p.41
- Bouvier J., Bertout C. 1989, A&A 211, 99
- Bouvier J., Bertout C., Bouchet P. 1986a, A&A 158, 149
- Bouvier J., Bertout C., Benz W., Mayor M. 1986b, A&A 165, 110
- Bouvier J., Cabrit C., Fernandez M., Martín E.L., Matthews J., in prep. (Paper I)
- Brown D.N., Landstreet T.D. 1981, ApJ 246, 899
- Cabrit S., Edwards S., Strom S.E., Strom K.M. 1990, ApJ 354, 687
- Calvet N., Hartmann L.W. 1992, ApJ 386, 239
- Camenzind M. 1990, Rev. Mod. Astron. 3
- Cameron A.C., Campbell C.G. 1992, A&A, in press
- Chen W.P., Simon M., Longmore A.J., Howell R.R., Benson J.A. 1990, ApJ 357, 224
- Cohen M., Kuhl L.V. 1979, ApJS 41, 743
- Dworetzky M.M. 1983, MNRAS 203, 917
- Edwards S., Ray T., Mundt R. 1992, in: Protostars and Planets III, eds. E. Levy & J. Lunine, in press
- Edwards S., Cabrit S., Strom S.E., Heyer I., Strom K.M., Anderson E. 1987, ApJ 321, 473
- Endal A.S., Sofia S. 1981, ApJ 243, 625
- Feigelson E.D., Jackson J.M., Mathieu R.D., Myers P.C., Walter F.M. 1987, AJ 94, 1251
- Ghez A.M., Neugebauer G., Gorham P.W., Haniff C.A. 1991, AJ 102, 2066
- Haas M., Leinert Ch., Zinnecker H. 1990, A&A 230, L1
- Hartmann L.W., Kenyon S.J. 1990, ApJ 349, 190
- Hartmann L.W., Stauffer J.R. 1989, AJ 97, 873
- Hartmann L.W., Soderblom D.R., Stauffer J.R. 1987, AJ 93, 907
- Hartmann L.W., Hewett R., Stahler S., Mathieu R.D. 1986, ApJ 309, 275
- Hartmann L.W., Jones B.F., Stauffer J.R., Kenyon S.J. 1991, AJ 101, 1050
- Herbig G.H. 1977, ApJ 214, 747
- Herbig G.H., Bell K.R. 1988, Lick Obs. Bull. No.1111
- Herbig G.H., Vrba F.J., Rydgren A.E. 1986, AJ 91, 575
- Herbst W. 1986, PASP 98, 1088
- Herbst W. et al. 1986, ApJ 310, L71
- Herbst W., Koret D.L. 1988, AJ 96, 1949
- Herbst W., Holtzman J.A., Phelps B.E. 1982, AJ 87, 1710
- Herbst W. et al. 1987, AJ 94, 137
- Holtzman J.A., Herbst W., Booth J. 1986, AJ 92, 1387
- Horne J.H., Baliunas S.L. 1986, ApJ 302, 757
- Joncour I., Bertout C. 1993, in prep.
- Joy A.H. 1949, ApJ 110, 424
- Kardopulov V.I. 1989, Astron. Tsirk., 1537, 23
- Kenyon S.J., Hartmann L.W. 1987, ApJ 323, 714
- Kraft R.P. 1967, ApJ 150, 551
- Königl A. 1991, ApJ 370, L39
- Leinert Ch., Haas M. 1989, ApJ 342, L39
- Leinert C., Haas M., Richichi A., Zinnecker H., Mundt R. 1991, A&A 250, 407
- Leinert C. et al. 1992, in: Complementary Approaches to Double and Multiple Star Research, IAU Coll. no.135, in press
- Libbrecht K.G. 1989, ApJ 336, 1092
- MacGregor K.B. 1991, in: Angular Momentum Evolution of Young Stars, eds. S. Catalano & J.R. Stauffer, p.315
- Magazzù A., Rebolo R., Pavlenko Y.V. 1992, ApJ, in press
- Martín E.L. 1992, PASP, submitted
- Mathieu R.D., Walter F.M., Myers P.C. 1989, AJ 98, 987
- Montmerle T., Koch-Miramond L., Falgarone E., Grindlay J.E. 1983, ApJ 269, 182
- Pinsonneault M.H., Kawaler S.D., Demarque P. 1990, ApJS 74, 501
- Pinsonneault M.H., Kawaler S.D., Sofia S., Demarque P. 1989, ApJ 338, 424
- Prosser C.F. 1991, Ph.D. Dissertation, Univ. Calif. Santa Cruz
- Reipurth B., Zinnecker H. 1992, A&A, submitted
- Rydgren A.E., Vrba F.J. 1983, ApJ 267, 191
- Rydgren A.E., Zak D.S., Vrba F.J., Chugainov P.F., Zajtseva G.V. 1984, AJ 89, 1015
- Schatzman E. 1962, Ann. d'Ap. 25, 18
- Shevchenko V.S. et al. 1991, Inf. Bul. Var. St., in press
- Simon M., Chen W.P., Howell R.R., Benson J.A., Slowik D. 1992, ApJ 384, 212
- Simon T., Vrba F.J., Herbst W. 1990, AJ 100, 1957
- Skrutskie M.F., Dutkevitch D., Strom S.E., Edwards S., Strom K.M., Shure M.A. 1990, AJ 99, 1187
- Skumanich A. 1972, ApJ 171, 565
- Stauffer J.R., Hartmann L.W. 1987, ApJ 318, 337
- Stauffer J.R., Soderblom D.R. 1991, in: The Sun in Time, eds. C.P. Sonnet, M.S. Giampapa, M.S. Matthews, p.832
- Stauffer J.R., Hartmann L.W., Jones B.F. 1989a, ApJ 346, 160
- Stauffer J.R., Hartmann L.W., Jones B.F., McNamara B.R. 1989b, ApJ 342, 285
- Strom K.M., Wilkin F.P., Strom S.E., Seaman R.L. 1989b, AJ 98, 1444
- Strom K.M., Strom S.E., Edwards S., Cabrit S., Skrutskie M.F. 1989a, AJ 97, 1451
- Torres C.A.O., Ferraz Mello S. 1973, A&A 27, 231
- Van Leeuwen F., Alphenaar P. 1982, The ESO Messenger, Vol.28, p.15
- Vogel S.N., Kuhl L.V. 1981, ApJ 245, 960
- Vogt S.S. 1981, ApJ 250, 327
- Vrba F.J., Herbst W., Booth J.F. 1988, AJ 96, 1032
- Vrba F.J., Rydgren A.E., Chugainov P.F., Shakovskaya N.I., Weaver W.B. 1989, AJ 97, 483
- Vrba F.J., Rydgren A.E., Chugainov P.F., Shakovskaya N.I., Zak D.S. 1986, ApJ 306, 199
- Walker M.F. 1987, PASP 99, 392
- Walter F.M. et al. 1987, ApJ 314, 297
- Walter F.M., Skinner S.L., Boyd W.T. 1990, PASP 102, 754
- Walter F.M., Wolk S., Vrba F.J., Brown A. 1992, in: Cool Stars, Stellar Systems and the Sun VII, eds. M.S. Giampapa & J. Bookbinder, in press
- Walter F.M., Brown A., Mathieu R.D., Myers P.C., Vrba F.J. 1988, AJ 96, 297
- Weaver W.B., Hobson S.W. 1988, PASP 100, 1443

This article was processed by the author using Springer-Verlag L<sup>A</sup>T<sub>E</sub>X A&A style file version 3.